levels in the absence of E_2 are represented as the average ± SD from three independent experiments.

Next, BCRP pulse-chase labeling was done without E_2 pretreatment, because ^{35}S-labeled BCRP was hardly detectable and the half-life of BCRP could not be determined in MCF-7/BCRP cells pretreated with E_2 for 4 days. Cells (2.5×10^6/well) were cultured in PRF-medium for 2 days and the resulting 70% to 80% confluent cells were incubated in labeling medium for 1.5 hours just before beginning the experiment, and then incubated in labeling medium containing 300 μCi/mL of [^{35}S] for 1 hour. The labeling medium was then replaced with fresh PRF-medium and the cells were lysed after 12, 24, 36, and 48 hours from the start of metabolic labeling. To investigate the effect of E_2 on BCRP stability, 3 nmol/L of E_2 was added to the medium in one set of the experiment and was present throughout the pulse-chase experiments. The subsequent procedure was the same as described for E_2-pretreated cells, except that one-fifth of the total immunoprecipitated protein was subjected to SDS-PAGE and autoradiography. The intensities of the bands representing metabolically labeled BCRP were quantified with the NIH-Image densitometric program. The BCRP half-life under each set of experimental conditions is represented as the average ± SD from three independent experiments.

Statistical Analysis. Statistical significance between the two sets of data was evaluated by using the two-sided unpaired Student's *t* test.

Results

Effects of Estrogens on Endogenous BCRP Expression. Effects of estrogens on endogenous BCRP expression were investigated by Western blotting under nonreducing conditions, as this generates stronger BCRP signals. Under the nonreducing conditions, BCRP was detected as a dimer of 160 kDa. Endogenous BCRP protein expression in MCF-7 cells decreased in a dose-dependent manner following treatment with E_1, E_2, and diethylstilbestrol (Fig. 1*A*). Both E_2 E_2 and diethylstilbestrol showed stronger suppressive effects on BCRP expression than E_1 did. MCF-7 cells expressed approximately 2-fold, 5-fold, and 10-fold less amounts of endogenous BCRP protein after treatment with 3 nmol/L E_2 for 1, 2, and 4 days, respectively, as compared with untreated MCF-7 cells (Fig. 1*B*). The inhibitory effect of estrogens on endogenous BCRP expression in MCF-7 cells was also observed in other MCF-7 clones (data not shown). In contrast, endogenous BCRP protein expression was not affected by E_2 in A549 cells (Fig. 1*A*). Because MCF-7 cells are ERα-positive and estrogen-responsive but A549 cells are ERα-negative (Fig. 1*C*), these results suggest that estrogen-mediated BCRP down-regulation might depend on signaling pathways downstream of ERα.

Effects of E_2 on Exogenous BCRP Expression in *BCRP*-Transduced Cells. We further studied the effects of E_2 on exogenous BCRP expression, driven by a constitutive long terminal repeat promoter, in MCF-7/BCRP, T-47D/BCRP, MDA-MB-231/BCRP, and SKOV-3/BCRP cells. Western blotting was done under both nonreducing and reducing conditions, in which BCRP was detected as a dimer of 160 kDa and as a monomer of 80 kDa, respectively. Exogenous BCRP expression decreased in MCF-7/BCRP and T-47D/BCRP cells in a dose-dependent manner following treatment with physiologic levels of E_2 (Fig. 2*A*). MCF-7/BCRP cells expressed approximately 2-fold, 4-fold, and 8-fold less amounts of exogenous BCRP protein after treatment with 3 nmol/L E_2 for 2, 3, and 4 days, respectively, as compared with untreated MCF-7/BCRP cells (Fig. 2*B*). In contrast, exogenous BCRP expression was not affected by E_2 treatment in MDA-MB-231/BCRP and SKOV-3/BCRP cells (Fig. 2*A*). MCF-7 and T-47D cells are estrogen-responsive and express functional ERα (Fig. 2*C*),

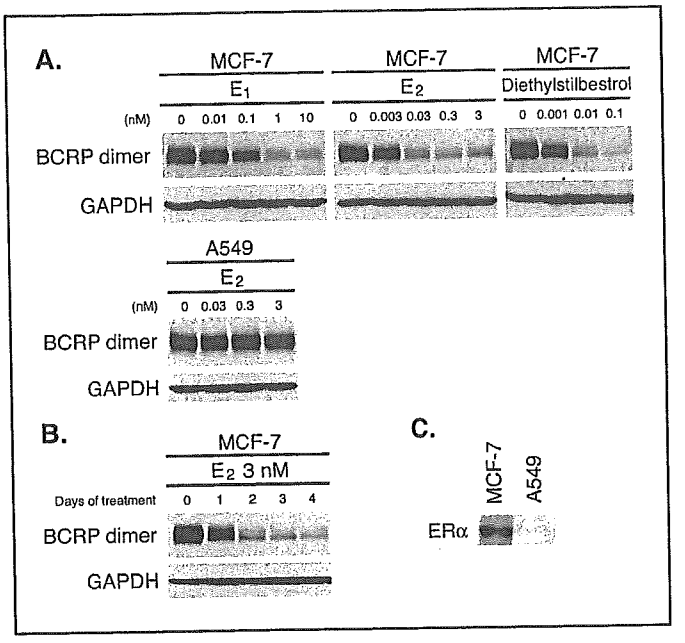

Figure 1. Effects of estrogens on endogenous BCRP expression in cancer cells. Cells were cultured in PRF-medium in the absence or presence of the indicated concentrations of estrogens for 4 days prior to harvesting. Western blot analysis was done under nonreducing conditions, such that the dimeric form of BCRP was detected as a band of approximately 160 kDa. Protein sample (30 μg) was loaded in each lane. BCRP was detected using the anti-BCRP monoclonal antibody, BXP-21. For ERα expression analysis, whole cell lysates consisting of 1.5×10^5 cells were loaded in each lane, and expression was detected by Western blotting using the anti-ERα monoclonal antibody, NCL-ER-6F11. To see how soon the E_2-mediated BCRP down-regulation occurs, MCF-7 cells were cultured for 1, 2, 3, and 4 days in PRF-medium in the presence of 3 nmol/L E_2. The following procedure was the same as described above. *A*, effects of estrogens on endogenous BCRP expression in MCF-7 cells and A549 cells. GAPDH expression was analyzed as a loading control. *B*, time course of E_2-mediated down-regulation of endogenous BCRP in MCF-7 cells. *C*, ERα expression in MCF-7 and A549 cells. The data are representative of at least three independent experiments.

whereas MDA-MB-231 cells do not express ERα, and SKOV-3 cells, which only weakly express nonfunctional ERα, are estrogen-nonresponsive (Fig. 2C; refs. 11, 12). These results also suggested that estrogen-mediated BCRP down-regulation may be dependent on ERα function, which may influence posttranscriptional processes rather than the transcription of *BCRP*.

E_2-mediated BCRP down-regulation was more remarkable in MCF-7/BCRP cells than in T-47D/BCRP cells, although MCF-7 cells and T-47D cells expressed similar amounts of ERα (Fig. 2). E_2-mediated BCRP down-regulation would therefore be affected not only by ERα expression levels but by other factors, such as signaling pathways downstream of ERα, in estrogen-responsive, ERα-positive cells.

Cell Growth Studies. E_2, at concentrations of 3×10^{-4} nmol/L or higher, induces mitogenic activity in MCF-7 and MCF-7/BCRP cells cultured in PRF-medium (Fig. 3*A-1*). The mitogenic activity saturated at concentrations of 0.03 nmol/L E_2 or higher in both cell types (Fig. 3*A-1*). The effects of E_2 on anticancer drug sensitivity were therefore investigated within this concentration range. At a concentration of 3 nmol/L, when compared with a 0.03 nmol/L dose, E_2 was found to marginally potentiate the cytotoxicity of SN-38, but not vincristine, in MCF-7 cells (Fig. 3*A-2*). The IC_{50} values for vincristine in the presence of 0.03 and 3 nmol/L E_2 were 0.69 ± 0.01 and 0.65 ± 0.02 nmol/L in MCF-7 cells, respectively. For SN-38, IC_{50} values in the presence of 0.03 and 3 nmol/L E_2

were 1.56 ± 0.15 and 1.22 ± 0.05 nmol/L in MCF-7 cells, respectively. Furthermore, exposure to 3 nmol/L E_2 significantly potentiated the cytotoxicity of SN-38, but not vincristine, in comparison to 0.03 nmol/L E_2 treatment in MCF-7/BCRP cells (Fig. 3*A-2*). The IC_{50} values for vincristine in the presence of 0.03 and 3 nmol/L E_2 were 0.74 ± 0.03 and 0.65 ± 0.02 nmol/L in MCF-7/BCRP cells, respectively. The IC_{50} values for SN-38 at a 3 nmol/L E_2 dose (2.65 ± 0.22 nmol/L) were significantly lower than the values at the 0.03 nmol/L E_2 dosage (5.18 ± 0.46 nmol/L; $P < 0.01$). Because mitogenic activity levels were saturated over the E_2 concentration range that was used (from 0.03 to 3 nmol/L), we conclude that these results also suggest E_2-mediated BCRP down-regulation in MCF-7/BCRP cells.

Intracellular Topotecan Uptake in MCF-7 and MCF-7/BCRP Cells. Effects of E_2 on cellular accumulation of topotecan were investigated. Cellular accumulation of topotecan increased in MCF-7 cells treated with 0.03 nmol/L E_2 as compared with untreated cells, whereas cellular accumulation of topotecan scarcely increased in MCF-7 cells treated with 3 nmol/L E_2 when compared with cells treated with 0.03 nmol/L E_2 (Fig. 3*B*). The results coincided with BCRP down-regulation in E_2-treated MCF-7 cells (Fig. 1*A*). As for MCF-7/BCRP cells, intracellular topotecan accumulation only marginally increased in the presence of 0.03 nmol/L E_2 as compared with untreated cells (Fig. 3*B*). Also, cellular accumulation of topotecan only marginally increased in MCF-7/BCRP cells treated with 3 nmol/L E_2 when compared with those treated with 0.03 nmol/L E_2 (Fig. 3*B*). The results suggest that down-regulation of exogenous BCRP in MCF-7/BCRP cells would not be enough for abrogation of topotecan efflux out of the cells, even after treatment xwith 3 nmol/L E_2.

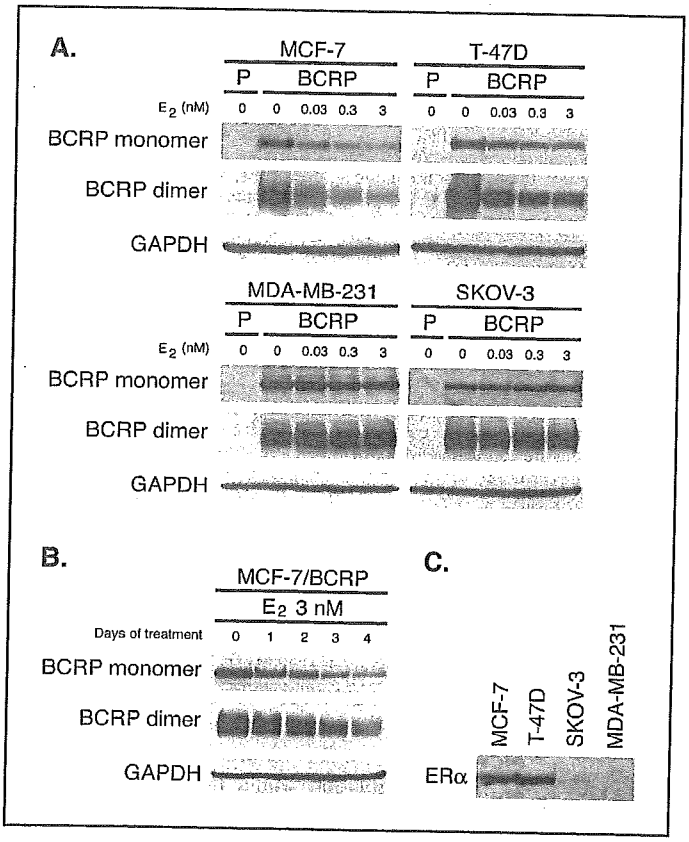

Figure 2. Effects of E_2 on exogenous BCRP expression in *BCRP*-transduced cancer cells. Cells were cultured in PRF-medium in the absence or presence of the indicated concentrations of E_2 for 4 days prior to harvesting. To see how soon the E_2-mediated BCRP down-regulation occurs, MCF-7/BCRP cells were cultured for 1, 2, 3, and 4 days in PRF-medium in the presence of 3 nmol/L E_2. The following procedure was the same as described above. *A*, Western blot analysis of exogenous BCRP expression. The monomeric form of BCRP was detected as an approximately 80 kDa band under reducing conditions, and the dimeric form of BCRP as an approximately 160 kDa band under nonreducing conditions. Protein sample (20 μg) was loaded in each lane. Exogenous BCRP tagged with c-*myc* was detected using anti-c-*myc* antibody, 9E10. GAPDH expression was analyzed as a loading control. *P* and *BCRP* indicate parental cells and *BCRP*-transduced cells, respectively. The data are representative of at least three independent experiments. *B*, time course of E_2-mediated down-regulation of exogenous BCRP in MCF-7/BCRP cells. *C*, ERα expression in MCF-7, T-47D, MDA-MB-231, and SKOV-3 cells. Whole cell lysates consisting of 1.5×10^5 cells were loaded in each lane. ERα expression was detected by Western blotting using the anti-ERα monoclonal antibody, NCL-ER-6F11.

Effects of Tamoxifen and ERα Knockdown by siRNA on E_2-mediated BCRP Down-regulation in MCF-7 and MCF-7/BCRP Cells. MCF-7 cells expressed similar amounts of endogenous BCRP in the presence of increasing concentrations of tamoxifen (Fig. 4*A*, *left*). In MCF-7/BCRP cells, marginally higher levels of exogenous BCRP were produced by increasing dosages of tamoxifen (Fig. 4*B*, *left*), possibly by competition with residual estrogens in the culture medium. Tamoxifen was also found to partially reverse the E_2-mediated down-regulation of either endogenous or exogenous BCRP in a dose-dependent manner (Fig. 4*A* and *B*, *right*). In these tamoxifen reversal experiments using MCF-7/BCRP cells, a concentration of 0.3 nmol/L E_2 was used to down-regulate BCRP, because tamoxifen even at levels of 0.5 μmol/L failed to reverse 3 nmol/L E_2-mediated BCRP down-regulation (data not shown). These results suggest that E_2-mediated BCRP down-regulation in MCF-7 and MCF-7/BCRP cells may be associated with the interaction of E_2 and ERα. We therefore did an experiment in which ERα expression was repressed using siRNA, and investigated the effects of this gene silencing on E_2-mediated modification of BCRP expression. Transfection of 100 nmol/L ERα siRNA resulted in a nearly complete loss of ERα expression in MCF-7/BCRP cells after 48 hours (Fig. 4*C-1*). In addition, this down-regulation of ERα expression persisted for at least 6 days after the siRNA transfections (data not shown). Gene silencing of ERα in MCF-7/BCRP cells by RNA interference was also found to attenuate E_2-mediated *BCRP* down-regulation (Fig. 4*C-2*), indicating that ERα is necessary for the repression of BCRP.

Semi-quantitative RT-PCR and Northern Blot Analysis of *BCRP* Expression in MCF-7 and MCF-7/BCRP Cells. RT-PCR and Northern blot analyses revealed that the treatment of MCF-7 cells with E_2 for 4 days did not affect the expression of endogenous *BCRP* mRNA (Fig. 5*A* and *B*, *left*). Similarly, the same treatment of MCF-7/BCRP cells with E_2 for 4 days did not affect exogenous *HaBCRP* mRNA levels (Fig. 5*B*, *right*). Considering that these treatments dramatically reduce BCRP protein expression levels (up to 10-20% of control levels following exposure to 3 nmol/L E_2), we speculated that the mechanism of E_2-mediated inhibition would be a posttranscriptional process.

Metabolic Labeling of BCRP in MCF-7/BCRP Cells. The biosynthesis and degradation of BCRP was further investigated by pulse-chase experiments. An outline of the experimental procedure is presented in Fig. 6*A*. MCF-7/BCRP cells produce a large amount of exogenous BCRP, driven by a constitutive long terminal repeat promoter, which could be successfully immunoprecipitated with the anti-BCRP antibody BXP-21, whereas the quantity of endogenous protein in parental MCF-7 cells is below the minimum detectable level (Fig. 6*B* and *C*). BCRP is initially detectable as a

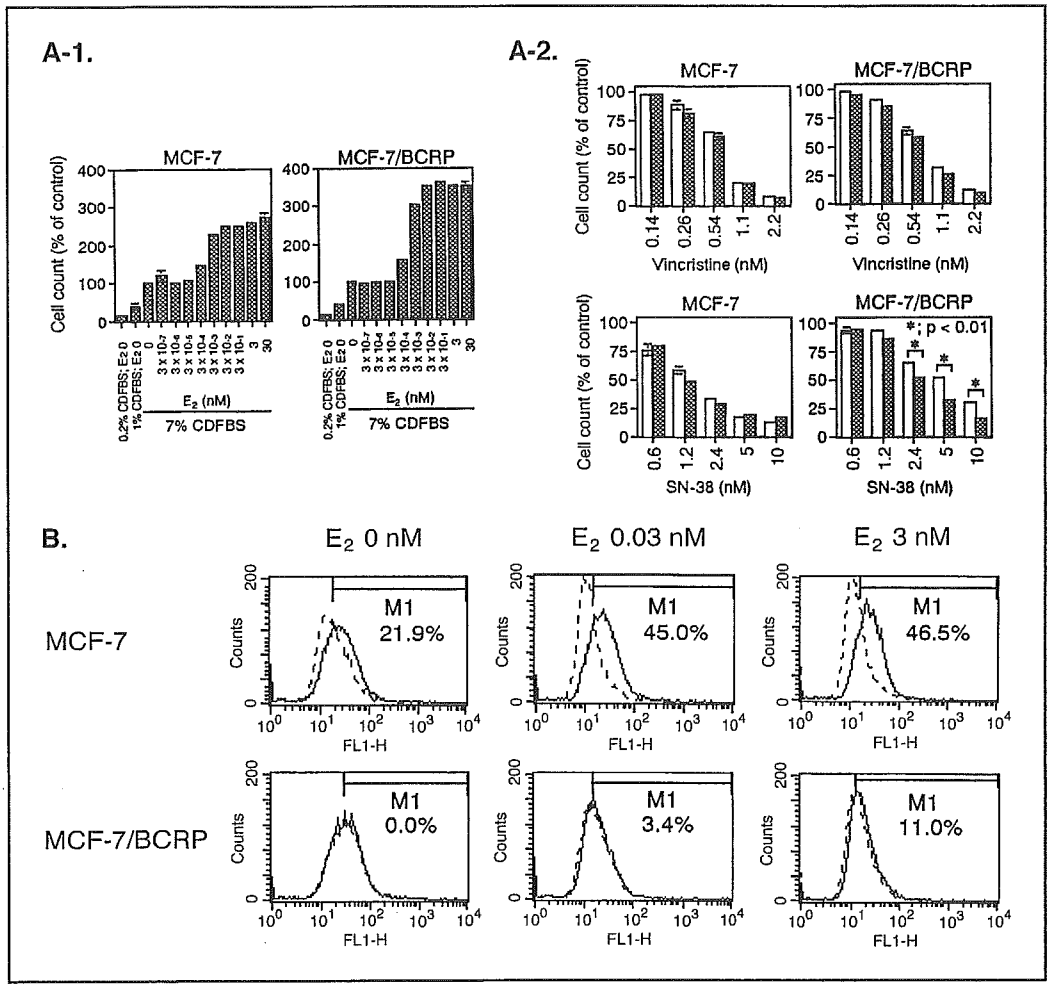

Figure 3. Cell growth studies and cellular topotecan uptake studies. *A*, cell growth studies. *A-1*, mitogenic effects of E_2 on MCF-7 and MCF-7/BCRP cells. Cells were cultured in PRF-DMEM supplemented with the indicated concentrations of CDFBS and E_2 for 4 days. Cell numbers were determined with a cell counter and presented as percentages relative to those of control cells cultured in PRF-medium. The given data are means ± SD of triplicate determinations. Invisible error bars are present within the symbols. The data are representative of two independent experiments. *A-2*, effects of E_2 on anticancer drug sensitivities in MCF-7 and MCF-7/BCRP cells. Cells were cultured in PRF-medium with 0.03 or 3 nmol/L E_2 for 4 days, and the cells (3×10^4) were then seeded into 12-well plates and cultured in PRF-medium with the same concentrations of E_2 used in pretreatments, in the absence or presence of increasing doses of specific anticancer agents for a further 4 days. Cell numbers were determined with a cell counter, and presented as percentages relative to those of control cells cultured in the absence of anticancer agents. *Clear columns*, cells cultured with 0.03 nmol/L E_2. *Dotted columns*, cells cultured with 3 nmol/L E_2. The given data are means ± SD of triplicate determinations, and are representative of three independent experiments. Where a vertical bar is not shown, the SD is within the bar. *, $P < 0.01$. *B*, effects of E_2 on cellular topotecan uptake. Cells were cultured in PRF-medium in the absence or presence of indicated concentrations of E_2 for 4 days. After trypsinization, cells (5×10^5) were incubated with (*solid line*) or without (*dotted line*) 20 μmol/L topotecan for 30 minutes. After washing, cellular uptake of topotecan was measured by fluorescence-activated cell sorting. Under each set of experimental conditions, 20,000 events were analyzed. Ratio (%) represents a fraction of topotecan-treated cells in the M1 area subtracted by that of control cells in the M1 area.

premature protein (66 kDa) which has a lower molecular size than the commonly observed *N*-glycosylated mature form (80 kDa; refs. 2, 13). During 1 hour of pulse labeling, the levels of mature protein gradually increased above the levels of the precursor molecule, and following 3 hours of chase period, only mature BCRP were measurable (Fig. 6*B*). Greater levels of metabolically labeled BCRP were observed in control MCF-7/BCRP cells, when compared with the E_2-treated cells, throughout the pulse-chase period (Fig. 6*B*). The relative rate of labeled BCRP at the 4-hour time point in the presence of 3 nmol/L E_2, over the levels measured in the absence of E_2, was 0.24 ± 0.01. Because metabolically labeled BCRP was only detectable at very low levels in E_2-treated cells and the half-life of synthesized BCRP could not be determined under these experimental conditions, the BCRP half-life was measured in cells without a 4-day E_2-pretreatment. E_2 (3 nmol/L) was added to the labeling medium and was present throughout the 48-hour pulse-chase period. The relative rate of labeled BCRP at the 1-hour time point in the presence of 3 nmol/L E_2, over the levels measured in the absence of E_2, was 0.84 ± 0.12. MCF-7/BCRP cells produced somewhat smaller amounts of labeled BCRP in the presence of 3 nmol/L E_2 than in the absence of E_2. The half-life of ^{35}S-labeled BCRP in the absence or presence of 3 nmol/L E_2 was similar, calculated as 35.6 ± 8.2 and 37.4 ± 6.3 hours, respectively (Fig. 6*C*). The relative rate of BCRP half-life in the presence of 3 nmol/L E_2 to that in the absence of E_2-treatment was 1.08 ± 0.27.

Discussion

We have recently reported several findings that provide evidence of interactions between BCRP and estrogens (6, 7, 14, 15). BCRP has been shown to export sulfated E_1, sulfated E_2, and genistein aglycone which has weak estrogenic activity (7, 15).

These data prompted us to investigate whether estrogens in fact regulate BCRP expression and we have now elucidated, contrary to our expectation that estrogens might augment BCRP expression, that physiologic levels of estrogens, such as E_1, E_2, and diethylstilbestrol, down-regulate BCRP expression in MCF-7 cells (Fig. 1).

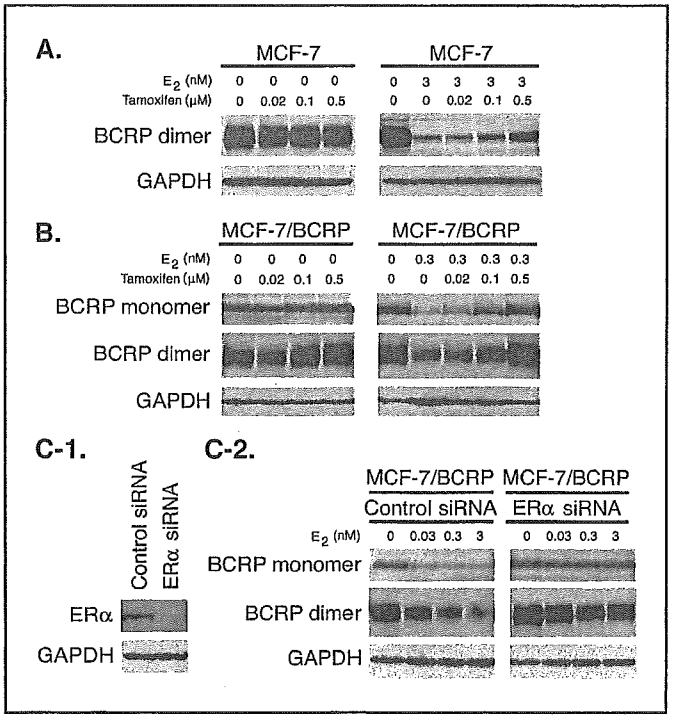

Figure 4. Effects of tamoxifen and ERα knockdown by RNA interference on E_2-mediated BCRP down-regulation. *A*, effects of tamoxifen on endogenous BCRP expression in MCF-7 cells. Cells were cultured in PRF-medium in the presence of indicated concentrations of compounds for 4 days prior to harvesting. Dimeric form of BCRP was detected as an approximately 160 kDa band under nonreducing conditions. Protein sample (30 μg) was loaded in each lane. Endogenous BCRP in MCF-7 cells was detected using the anti-BCRP antibody, BXP-21. *Left*, effects of tamoxifen on endogenous BCRP expression. *Right*, reversal effects of tamoxifen on E_2-mediated down-regulation of endogenous BCRP. GAPDH expression was analyzed as a loading control. The data are representative of two independent experiments. *B*, effects of tamoxifen on exogenous BCRP expression in MCF-7/BCRP cells. Cells were cultured in PRF-medium in the presence of the indicated concentrations of compounds for 4 days prior to harvesting. Dimeric form of BCRP was detected as an approximately 160 kDa band under nonreducing conditions, and the monomeric form of BCRP was detected as an approximately 80 kDa band under reducing conditions by Western blotting. Protein sample (20 μg) was loaded in each lane. Exogenous BCRP in MCF-7/BCRP cells was detected using the anti-c-*myc* antibody, 9E10. *Left*, effects of tamoxifen on exogenous BCRP expression. *Right*, reversal effects of tamoxifen on E_2-mediated down-regulation of exogenous BCRP. GAPDH expression was analyzed as a loading control. The data are representative of two independent experiments. *C*, effects of ERα knockdown by RNA interference on E_2-mediated BCRP down-regulation in MCF-7/BCRP cells. Cells (2.5×10^5/well) were cultured in PRF-medium in six-well plates for 24 hours and then transfected with 100 nmol/L of either control or ERα siRNA (SMARTpool GL3 Duplex for control; SMARTpool ESR1 for ERα) using LipofectAMINE 2000. To confirm ERα knockdown, the culture medium was exchanged with fresh PRF-medium 6 hours after transfection. After 48 hours, the cells were harvested and whole cell lysates consisting of 1.5×10^5 cells were loaded in each lane. ERα expression was detected by Western blotting using anti-ERα monoclonal antibody, NCL-ER-6F11. To examine the effects of ERα knockdown on E_2-mediated BCRP down-regulation, the culture medium was exchanged with fresh PRF-medium containing the indicated concentrations of E_2 6 hours after transfection. After 96 hours, cells were harvested and exogenous BCRP expression was examined by Western blotting as described above. *C-1*, siRNA-induced knockdown of ERα expression. *C-2*, effects of ERα knockdown on E_2-mediated BCRP down-regulation.

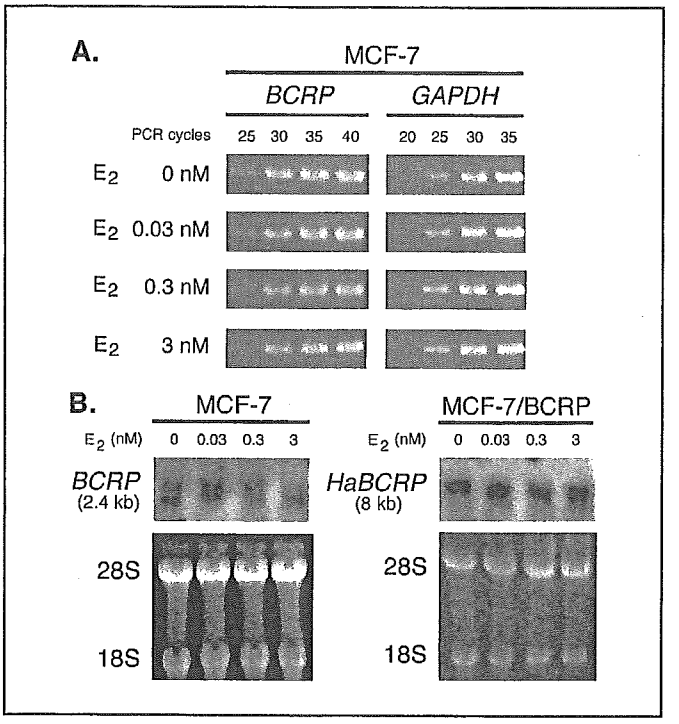

Figure 5. Expression analysis of *BCRP* mRNA in MCF-7 and MCF-7/BCRP cells. Cells were cultured in PRF-medium supplemented with the indicated concentrations of E_2 for 4 days. Exponentially growing cells were then harvested and total RNA was extracted. *A*, semi-quantitative RT-PCR of endogenous *BCRP* mRNA in MCF-7 cells. First-strand cDNA was synthesized with 0.3 μg of total RNA and a *BCRP* cDNA fragment (315 bp) was amplified by PCR using the indicated cycle numbers. Amplification of *GADPH* mRNA (551 bp fragment) was carried out as an internal control. The data are representative of two independent experiments. *B*, Northern blotting of endogenous *BCRP* mRNA in MCF-7 cells (*left*) and exogenous *HaBCRP* mRNA in MCF-7/BCRP cells (*right*). Either 20 μg (MCF-7) or 10 μg (MCF-7/BCRP) of total RNA was loaded in each lane. The blot was hybridized with a ^{32}P-labeled internal *BCRP* cDNA probe and then exposed to X-ray film for either 21 days (MCF-7) or 7 days (MCF-7/BCRP). Endogenous *BCRP* mRNA was detected as a band of approximately 2.4 kb in size, and exogenous *HaBCRP* mRNA as a band of approximately 8 kb in size. Under the experimental conditions used for MCF-7/BCRP cells, endogenous *BCRP* mRNA was not detected. Ethidium bromide staining of total RNA is presented as a loading control. *28s* and *18s*, 28S and 18S rRNA, respectively. The data are representative of two independent experiments.

Furthermore, E_2 strongly reduces the levels of exogenous BCRP in MCF-7/BCRP and T-47D/BCRP cells, the expression of which is constitutively transcribed by a Harvey long terminal repeat promoter (Fig. 2). Moreover, MCF-7/BCRP cells in the presence of 3 nmol/L E_2 were significantly more sensitive to SN-38, but not vincristine, than the same cells treated with 0.03 nmol/L E_2 (Fig. 3*A-2*). Because E_2 at a concentration ranging from 0.03 to 3 nmol/L shows similar mitogenic properties in MCF-7/BCRP cells (Fig. 3*A-1*), this further suggests that E_2 mediates the down-regulation of BCRP in these cells.

In proportion to BCRP down-regulation in MCF-7 cells, cellular accumulation of topotecan was found to increase by E_2-treatment (Fig. 3*B*). The increase in cellular topotecan uptake was most obvious when comparisons were made between untreated MCF-7 cells and MCF-7 cells treated with 0.03 nmol/L E_2. The results were coincident with BCRP protein expression levels in MCF-7 cells treated with E_2, in which BCRP down-regulation was most obvious when comparison was made between treatment with 0 nmol/L E_2 and that with 0.03 nmol/L E_2 (Fig. 1*A*). By contrast, the increase in cellular topotecan uptake was minimal even when untreated MCF-7/BCRP cells and MCF-7/BCRP cells treated with 3 nmol/L E_2 were

compared (Fig. 3*B*). Because exogenous BCRP synthesis levels in MCF-7/BCRP cells treated with 3 nmol/L E_2 are still greater than endogenous BCRP levels in E_2-untreated MCF-7 cells, we suppose that down-regulated BCRP by 3 nmol/L E_2 might still sufficiently efflux topotecan out of the cells (Fig. 6).

MCF-7 and T-47D cells are estrogen-responsive cells that express ERα, and it was significant that the estrogen-mediated down-regulation of endogenous BCRP was not observed in A549 cells, which do not express this receptor (Fig. 1). E_2-mediated down-regulation of exogenous BCRP was observed in MCF-7/BCRP and T-47D/BCRP cells, but not in MDA-MB-231/BCRP cells which also do not express ERα (Fig. 2*A*). Consistent with this, E_2-mediated BCRP repression was not observed in SKOV-3/BCRP cells (Fig. 2*A*), which express a small amount of nonfunctional ERα, possibly due to the disruption of downstream signaling pathways or an inactivating mutation within the ERα gene (11, 12). The antiestrogen drug tamoxifen partially reverses the E_2-mediated down-regulation of endogenous BCRP in MCF-7 cells and exogenous BCRP in MCF-7/BCRP cells (Fig. 4*A* and *B*). In addition, ERα knockdown by RNA interference in MCF-7/BCRP cells also abolishes the E_2-mediated down-regulation of exogenous BCRP (Fig. 4*C*). These results suggest that functional expression of ERα and the activity of its associated downstream pathways are important for estrogen-mediated BCRP down-regulation.

We first found that estrogens down-regulated BCRP expression at the protein level in MCF-7 cells (Fig. 1*A*). This was evident in experiments with three independent MCF-7 clones (data not shown). Subsequent semi-quantitative RT-PCR and Northern blotting analyses revealed that endogenous *BCRP* transcript levels were not reduced by E_2 treatment in MCF-7 cells (Fig. 5*A* and *B*, *left*). Furthermore, E_2 exposure decreased exogenous BCRP expression in MCF-7/BCRP and T-47D/BCRP cells, both constitutively expressing BCRP, driven by a Harvey long terminal repeat promoter. In addition, exogenous *HaBCRP* transcript levels were not reduced by E_2 treatment in MCF-7/BCRP cells (Fig. 5*B*, *right*). These data strongly argue for the existence of an estrogen-mediated posttranscriptional BCRP regulation mechanism, such as the degradation of translation products. We therefore did a pulse-chase experiment using MCF-7/BCRP cells. BCRP is a glycoprotein, containing four potential *N*-glycosylation sites (2, 13). BCRP was initially detectable as a premature protein of approximately 66 kDa in size at the 30-minute time point from the start of the pulse labeling, and a mature protein product of 80 kDa was then predominantly detected after 1 hour of the pulse labeling (Fig. 6*B*). In MCF-7/BCRP cells, the measured half-life of ^{35}S-labeled BCRP in the absence or presence of 3 nmol/L E_2 was similar, calculated as 35.6 ± 8.2 and 37.4 ± 6.3 hours, respectively (Fig. 6*C*). However, E_2-treated MCF-7/BCRP cells produced far smaller quantities of ^{35}S-labeled BCRP when compared with the control cells (Fig. 6*B*). In the pulse-chase experiments using MCF-7/BCRP cells pretreated with E_2 for 4 days before experiments, the ratio of mature BCRP at the 4-hour time point in the presence of 3 nmol/L E_2 to that in the absence of E_2 was 0.24 ± 0.01 (Fig. 6*B*). These results suggested that E_2 suppresses the biosynthesis of mature BCRP.

The sequence and characterization of the *BCRP* gene promoter has previously been reported (8). Very recently, an estrogen responsive element was identified in the *BCRP* promoter, and E_2-mediated activation of the *BCRP* promoter in a luciferase reporter system has been shown in ERα-negative ovarian cancer PA-1 cells, upon cotransfection with an ERα expression vector (9). In addition, E_2 has been shown to induce the increased expression of endogenous *BCRP* transcripts in T47D:A18 cells, established from T-47D cells by dilution cloning (9, 16). In our study, however, *BCRP* mRNA levels were unaffected by E_2 (Fig. 5*A* and *B*, *left*) and endogenous BCRP protein levels were clearly reduced in response to E_2 treatment in MCF-7 cells (Fig. 1*A*). Because T-47D cells

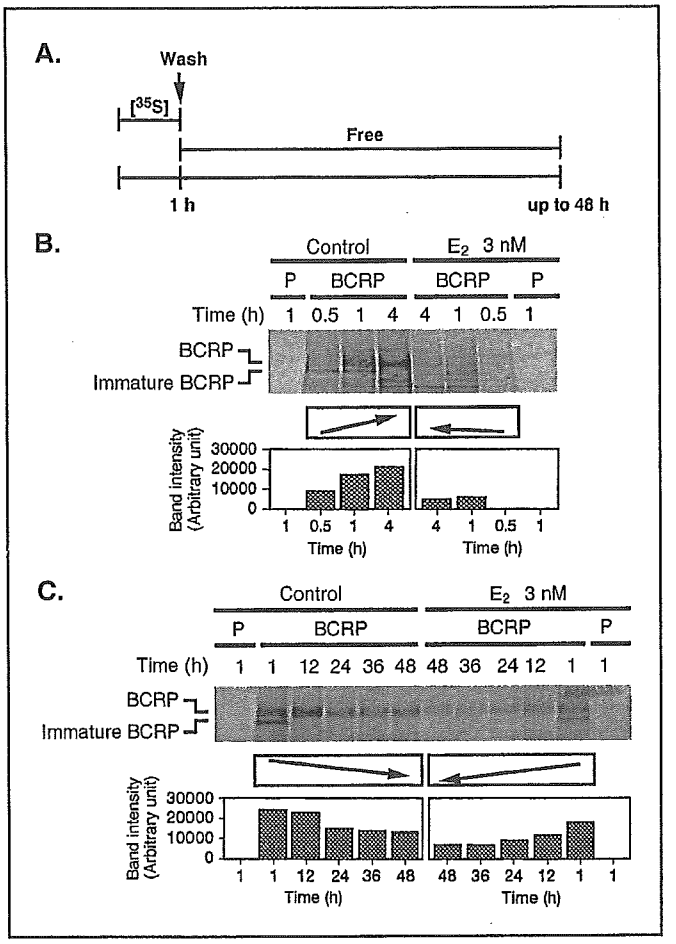

Figure 6. Metabolic labeling of BCRP in MCF-7/BCRP cells. *A*, an outline of the experimental procedure. *B*, biosynthesis of BCRP (0.5-4 h). Cells (1×10^6/well for control cells or 0.3×10^6/well for E_2-treated cells) were cultured in PRF-medium in a six-well plate for 4 days in the absence or presence of 3 nmol/L E_2. Exponentially growing cells were then incubated in methionine-free and cystine-free DMEM supplemented with 7% CDFBS (labeling medium) for 1.5 hours just prior to beginning the experiment. The cells were then metabolicallylabeled with 300 μCi/mL of [^{35}S] for both 0.5 and 1 hour periods. After 1 hour of pulse labeling, the labeling medium was replaced with fresh PRF-medium and the cells were chased for an additional 3 hours. For E_2-pretreated cells, 3 nmol/L E_2 was added to the medium and was present throughout the pulse-chase period. After preparation of cell lysates, ^{35}S-labeled BCRP was immunoprecipitated from 100 μg of the cell lysate with 0.5 μg BXP-21, subjected to SDS-PAGE, and autoradiographed. The band intensities representing metabolically labeled BCRP were quantified with NIH-Image. The data are representative of three independent experiments. *P* and *BCRP*, parental and MCF-7/BCRP cells, respectively. *C*, pulse-chase experiment of BCRP (1-48 h). Cells (2.5×10^6/well) were cultured in PRF-medium in six-well plates for 2 days. After incubation in labeling medium for 1.5 hours just before beginning the experiment, cells were metabolically labeled with 300 μCi/mL of [^{35}S] for 1 hour. The labeling medium was then replaced with fresh PRF-medium. The cells were lysed at 12, 24, 36, and 48 hours from the start of metabolic labeling. To investigate the effect of E_2 on BCRP stability, 3 nmol/L of E_2 was added to the medium in one set of experiments and was present in the medium throughout the pulse-chase periods. The following procedure in this case was identical to the one already described above, except that one-fifth of the total immunoprecipitated protein was subjected to SDS-PAGE and autoradiography. The band intensities, representing metabolically labeled BCRP, were quantified with NIH-Image. The data are representative of three independent experiments. *P* and *BCRP*, parental and MCF-7/BCRP cells, respectively.

express very low levels of endogenous BCRP, we could not examine the effect of E_2 on these levels by Western blotting. However, E_2 clearly reduced exogenous BCRP protein expression, which was driven by a constitutive promoter, in T-47D/BCRP cells (Fig. 2*A*), probably by inhibiting the biosynthesis of BCRP. Thus, E_2 up-regulates BCRP via transcriptional activation in some T-47D cells (T47D:A18 cells), and E_2 down-regulates BCRP expression via posttranscriptional mechanisms in some T-47D cells (T-47D/BCRP cells). Although both T47D:A18 cells and T-47D/BCRP cells were established from T-47D cells obtained from the same supplier, T47D:A18 cells were established by dilution cloning after repeated passages and T-47D/BCRP cells, a mixed population of stable *BCRP*-transduced cells, were used for the experiments shortly after supplied (16). The factors underlying distinct E_2-mediated BCRP regulation between these two T-47D derived cells remain to be elucidated.

Based upon global analyses of estrogen responsive genes in MCF-7 cells by cDNA microarray, many of these factors were determined to be growth- or transcription-related genes but no genes associated with protein translation have thus far been identified (17, 18). Among the candidate genes in these microarray screens, quiescin Q6, a FAD-dependent sulfhydryl oxidase, was reported to be estrogen-repressed (17). Quiescin Q6 products are expressed in the endoplasmic reticulum, Golgi, and extracellular spaces, and catalyze disulfide-bond formation in specific proteins (19, 20). Although it is currently unknown whether this protein interacts with BCRP, the maturation of BCRP by dimerization through bridge formation by disulfide bonds might well be necessary for stable BCRP expression. In addition, impaired protein maturation (glycosidation) or trafficking may also cause early degradation of the BCRP protein, as shown for multidrug resistance-related protein 2 (21, 22). Undetermined proteins associated with maturation or trafficking may also have caused very early degradation of premature BCRP.

BCRP had been initially isolated as an overexpressed protein in drug-resistant MCF-7 variants, but its expression is rarely observed in breast cancer cells (2, 23–25). The lack of BCRP protein expression notwithstanding high *BCRP* mRNA levels in nine breast cancer samples has also been previously reported (24). The authors of this study discussed whether this discrepancy might be due to the contribution of nontumor lactiferous ducts and blood vessels, both expressing BCRP, included in the tumor samples. However, we speculate that the low levels of BCRP protein in breast cancer cells might be explained by the inhibition of protein biosynthesis because a majority of primary breast cancers express ERα (26).

BCRP has been implicated in the cellular transport of several organic compounds (15, 27–29), and we have previously shown that it transports sulfated estrogens (7). Because mammary glands are one of the target organs of estrogens, we reasoned that BCRP in mammary glands might export sulfated estrogens and that, accordingly, estrogens may enhance its expression levels. MCF-7 cells also inactivate estrogens by sulfate conjugation (data not shown), and BCRP would most likely efflux them out of the cells. Moreover, it has been recently reported that BCRP expression was decreased in MCF-7 cells maintained in low folate medium (30). Because BCRP has been shown to transport methotrexate using membrane vesicle transport assays, the finding that BCRP expression is down-regulated was not considered to be surprising. However, in the case of estrogen treatment, this did not increase but considerably decreased BCRP expression in MCF-7 cells. Estrogen-mediated regulation of BCRP might therefore be responsible for the accumulation of estrogen in breast cancer cells.

In conclusion, our findings in this study show that estrogen posttranscriptionally decreases BCRP expression in estrogen-responsive cancer cells. This is also the first report showing that small molecules could modulate BCRP expression in cells, and our data therefore provide new insights into the regulation of BCRP expression and may assist in establishing new strategies for the reversal of BCRP-mediated multidrug resistance.

Acknowledgments

Received 8/10/2004; revised 10/27/2004; accepted 11/9/2004.

Grant support: The Ministry of Education, Culture, Sports, Science and Technology, and the Ministry of Health, Labor, and Welfare, Japan. The Hishinomi Cancer Research Fund, and the Virtual Research Institute of Aging of Nippon, Boehringer Ingelheim, Japan.

The cost of publication of this article were defrayed in part by the payment of page charges. This article must therefore be hereby marked advertisement in accordance with 18 U.S.C. Section 1734 solely to indicate this fact.

References

1. Allikmets R, Schriml L, Hutchinson A, Romano-Spica V, Dean M. A human placenta-specific ATP-binding cassette gene (*ABCP*) on chromosome 4q22 that is involved in multidrug resistance. Cancer Res 1998; 58:5337–9.
2. Doyle LA, Yang W, Abruzzo LV, et al. A multidrug resistance transporter from human MCF-7 breast cancer cells. Proc Natl Acad Sci U S A 1998;95:15665–70.
3. Miyake K, Mickley L, Litman T, et al. Molecular cloning of cDNAs which are highly overexpressed in mitoxantrone-resistant cells: demonstration of homology to ABC transport genes. Cancer Res 1999;59:8–13.
4. Maliepaard M, van Gastelen MA, de Jong LA, et al. Overexpression of the *BCRP/MXR/ABCP* gene in a topotecan-selected ovarian tumor cell line. Cancer Res 1999;59:4559–63.
5. Kawabata S, Oka M, Shiozawa K, et al. Breast cancer resistance protein directly confers SN-38 resistance of lung cancer cells. Biochem Biophys Res Commun 2001;280:1216–23.
6. Imai Y, Tsukahara S, Ishikawa E, Tsuruo T, Sugimoto Y. Estrone and 17β-estradiol reverse breast cancer resistance protein-mediated multidrug resistance. Jpn J Cancer Res 2002;93:231–5.
7. Imai Y, Asada S, Tsukahara S, Ishikawa E, Tsuruo T, Sugimoto Y. Breast cancer resistance protein exports sulfated estrogens but not free estrogens. Mol Pharmacol 2003;64:610–8.
8. Bailey-Dell KJ, Hassel B, Doyle LA, Ross DD. Promoter characterization and genomic organization of the human breast cancer resistance protein (ATP-binding cassette transporter G2) gene. Biochim Biophys Acta 2001;1520:234–41.
9. Ee PL, Kamalakaran S, Tonetti D, He X, Ross DD, Beck WT. Identification of a novel estrogen response element in the breast cancer resistance protein (ABCG2) gene. Cancer Res 2004;64:1247–1.
10. Kage K, Tsukahara S, Sugiyama T, et al. Dominant-negative inhibition of breast cancer resistance protein as drug efflux pump through the inhibition of S-S dependent homodimerization. Int J Cancer 2002; 97:626–30.
11. Hua W, Christianson T, Rougeot C, Rochefort H, Clinton GM. SKOV3 ovarian carcinoma cells have functional estrogen receptor but are growth-resistant to estrogen and antiestrogens. J Steroid Biochem Mol Biol 1995;55:279–89.
12. Lau KM, Mok SC, Ho SM. Expression of human estrogen receptor-α and -β, progesterone receptor, and androgen receptor mRNA in normal and malignant ovarian epithelial cells. Proc Natl Acad Sci U S A 1999;96:5722–7.
13. Maliepaard M, Scheffer GL, Faneyte IF, et al. Subcellular localization and distribution of the breast cancer resistance protein transporter in normal human tissues. Cancer Res 2001;61:3458–64.
14. Sugimoto Y, Tsukahara S, Imai Y, et al. Reversal of breast cancer resistance protein-mediated drug resistance by estrogen antagonists and agonists. Mol Cancer Ther 2003;2:105–12.
15. Imai Y, Tsukahara S, Asada S, Sugimoto Y. Phytoestrogens/flavonoids reverse breast cancer resistance protein/ABCG2-mediated multidrug resistance. Cancer Res 2004;64:4346–52.

16. Murphy CS, Pink JJ, Jordan VC. Characterization of a receptor-negative, hormone-nonresponsive clone derived from a T47D human breast cancer cell line kept under estrogen-free conditions. Cancer Res 1990;50: 7285–92.
17. Inoue A, Yoshida N, Omoto Y, et al. Development of cDNA microarray for expression profiling of estrogen-responsive genes. J Mol Endocrinol 2002;29:175–92.
18. Coser KR, Chesnes J, Hur J, Ray S, Isselbacher KJ, Shioda T. Global analysis of ligand sensitivity of estrogen inducible and suppressible genes in MCF7/BUS breast cancer cells by DNA microarray. Proc Natl Acad Sci U S A 2003;100:13994–9.
19. Benayoun B, Esnard-Feve A, Castella S, Courty Y, Esnard F. Rat seminal vesicle FAD-dependent sulfhydryl oxidase. Biochemical characterization and molecular cloning of a member of the new sulfhydryl oxidase/quiescin Q6 gene family. J Biol Chem 2001;276:13830–7.
20. Thorpe C, Hoober KL, Raje S, et al. Sulfhydryl oxidases: emerging catalysts of protein disulfide bond formation in eukaryotes. Arch Biochem Biophys 2002;405:1–12.
21. Keitel V, Kartenbeck J, Nies AT, Spring H, Brom M, Keppler D. Impaired protein maturation of the conjugate export pump multidrug resistance protein 2 as a consequence of a deletion mutation in Dubin-Johnson syndrome. Hepatology 2000;32:1317–28.
22. Hashimoto K, Uchiumi T, Konno T, et al. Trafficking and functional defects by mutations of the ATP-binding domains in MRP2 in patients with Dubin-Johnson syndrome. Hepatology 2002;36:1236–45.
23. Scheffer GL, Maliepaard M, Pijnenborg AC, et al. Breast cancer resistance protein is localized at the plasma membrane in mitoxantrone- and topotecan-resistant cell lines. Cancer Res 2000;60:2589–93.
24. Faneyte IF, Kristel PM, Maliepaard M, et al. Expression of the breast cancer resistance protein in breast cancer. Clin Cancer Res 2002;8:1068–74.
25. Diestra JE, Scheffer GL, Catala I, et al. Frequent expression of the multi-drug resistance-associated protein BCRP/MXR/ABCP/ABCG2 in human tumours detected by the BXP-21 monoclonal antibody in paraffin-embedded material. J Pathol 2002;198:213–9.
26. McGuire WL, Chamness GC, Costlow ME, Richert NJ. Steroids and human breast cancer. J Steroid Biochem Mol Biol 1975;6:723–7.
27. Zhou S, Schuetz JD, Bunting KD, et al. The ABC transporter Bcrp1/ABCG2 is expressed in a wide variety of stem cells and is a molecular determinant of the side-population phenotype. Nat Med 2001;7:1028–34.
28. Jonker JW, Buitelaar M, Wagenaar E, et al. The breast cancer resistance protein protects against a major chlorophyll-derived dietary phototoxin and protoporphyria. Proc Natl Acad Sci U S A 2002;99:15649–54.
29. van Herwaarden AE, Jonker JW, Wagenaar E, et al. The breast cancer resistance protein (Bcrp1/Abcg2) restricts exposure to the dietary carcinogen 2-amino-1-methyl-6-phenylimidazo[4,5-b]pyridine. Cancer Res 2003;63:6447–52.
30. Ifergan I, Shafran A, Jansen G, Hooijberg JH, Scheffer GL, Assaraf YG. Folate deprivation results in the loss of breast cancer resistance protein (BCRP/ABCG2) expression: A role for BCRP in cellular folate homeostasis. J Biol Chem 2004;279:25527–34.

p53-Defective Tumors With a Functional Apoptosome-Mediated Pathway: A New Therapeutic Target

Tetsuo Mashima, Tomoko Oh-hara, Shigeo Sato, Mikiko Mochizuki, Yoshikazu Sugimoto, Kanami Yamazaki, Jun-ichi Hamada, Mitsuhiro Tada, Tetsuya Moriuchi, Yuichi Ishikawa, Yo Kato, Hiroshi Tomoda, Takao Yamori, Takashi Tsuruo

Background: **Although cancer cells appear to maintain the machinery for intrinsic apoptosis, defects in the pathway develop during malignant transformation, preventing apoptosis from occurring. How to specifically induce apoptosis in cancer cells remains unclear.** ***Methods:*** **We determined the apoptosome activity and p53 status of normal human cells and of lung, colon, stomach, brain, and breast cancer cells by measuring cytochrome c–dependent caspase activation and by DNA sequencing, respectively, and we used COMPARE analysis to identify apoptosome-specific agonists. We compared cell death, cytochrome c release, and caspase activation in NCI-H23 (lung cancer), HCT-15 (colon cancer), and SF268 (brain cancer) cells treated with Triacsin c, an inhibitor of acyl-CoA synthetase (ACS), or with vehicle. The cells were mock, transiently, or stably transfected with genes for Triacsin c–resistant ACSL5, dominant negative caspase-9, or apoptotic protease activating factor-1 knockdown. We measured ACS activity and levels of cardiolipin, a mitochondrial phospholipid, in mock and ACSL5-transduced SF268 cells. Nude mice carrying NCI-H23 xenograft tumors (n = 10) were treated with Triacsin c or vehicle, and xenograft tumor growth was assessed. Groups were compared using two-sided Student *t* tests.** ***Results:*** **Of 21 p53-defective tumor cell lines analyzed, 17 had higher apoptosome activity than did normal cells. Triacsin c selectively induced apoptosome-mediated death in tumor cells (caspase activity of Triacsin c–treated versus untreated SF268 cells; means = 1020% and 100%, respectively; difference = 920%, 95% CI = 900% to 940%; $P<.001$). Expression of ACSL5 suppressed Triacsin c–induced cytochrome c release and subsequent cell death (cell survival of Triacsin c–treated mock- versus ACSL5-transduced SF268 cells; means = 40% and 83%, respectively; difference = 43%, 95% CI = 39% to 47%; $P<.001$). ACS was also essential to the maintenance of cardiolipin levels. Finally, Triacsin c suppressed growth of xenograft tumors (relative tumor volume on day 21 of Triacsin c–treated versus untreated mice; means = 4.6 and 9.6, respectively; difference = 5.0, 95% CI = 2.1 to 7.9; $P = .006$).** ***Conclusions:*** **Many p53-defective tumors retain activity of the apoptosome, which is therefore a potential target for cancer chemotherapy. Inhibition of ACS may be a novel strategy to induce the death of p53-defective tumor cells. [J Natl Cancer Inst 2005;97:765–77]**

Apoptosis is a genetically regulated process with central roles in tissue development and homeostasis *(1)*. Apoptosis signals are altered in many human diseases, including cancer. Various types of stress induce apoptosis through the intrinsic pathway, which involves the release of cytochrome c from the mitochondria *(2)*. The liberated cytochrome c binds to apoptotic protease activating factor-1 (apaf-1), which subsequently assembles into an oligomer termed the apoptosome. The apoptosome recruits and activates caspase-9, which subsequently activates a proteolytic cascade that ultimately results in cell death. The p53 tumor suppressor plays an essential role in transducing the apoptosis signal. p53 is

Affiliations of authors: Cancer Chemotherapy Center, Japanese Foundation for Cancer Research, Tokyo, Japan (T. Mashima, TO, SS, MM, YS, KY, TY, TT); Division of Cancer-Related Genes, Institute for Genetic Medicine, Hokkaido University School of Medicine, Sapporo, Japan (T. Moriuchi, JH, MT); Cancer Institute, Japanese Foundation for Cancer Research, Tokyo, Japan (YI, YK); Kitasato Institute for Life Sciences & Graduate School of Infection Control Sciences, Kitasato University, Tokyo, Japan (HT); Department of Chemotherapy, Kyoritsu University of Pharmacy, Tokyo, Japan (YS); Institute of Molecular and Cellular Biosciences, the University of Tokyo, Tokyo, Japan (TT).

Correspondence to: Takashi Tsuruo, PhD, Cancer Chemotherapy Center, Japanese Foundation for Cancer Research, 3–10–6 Ariake, Koutou-ku, Tokyo, Japan 135–8550 (e-mail: ttsuruo@iam.u-tokyo.ac.jp).

See "Notes" following "References."

DOI: 10.1093/jnci/dji133

Journal of the National Cancer Institute, Vol. 97, No. 10, © Oxford University Press 2005, all rights reserved.

a transcription factor that regulates the expression of multiple apoptosis-inducing proteins that act on the mitochondria, such as bax, noxa, puma, and p53AIP1 *(3)*.

In cancer cells, excessive mitotic signals, including oncogene-dependent signals and signals that trigger cell cycle progression, activate the intrinsic pathway *(4)*. For example, the expression of both apaf-1 and caspases is transcriptionally upregulated by E2F, a transcription factor that is essential for cell cycle progression that is often upregulated in cancer cells *(5,6)*, and the overexpression of apaf-1 and caspases in tumors has been reported *(7,8)*. Another cell cycle factor, cyclin D3, also activates caspase-2 *(9)*. These observations indicate that the intrinsic apoptosis machinery is active in tumors and that it could be a target for selectively killing cancer cells. Indeed, recent reports have shown that tumor cells, but not normal cells, are preferentially sensitive to agents that directly activate the apoptosome *(10)* or target the mitochondria *(11)*.

In contrast to the notion that the intrinsic apoptosis pathway is active in cancer cells, proapoptotic signals generated by an oncogene, by DNA damage, or by depletion of survival factors can also act as selection pressures, and, to acquire a survival advantage, cells develop defects in the apoptosis pathway during malignant transformation *(12,13)*. In fact, the p53 tumor suppressor is inactivated in more than half of human tumors. Recent studies further indicate that defects in the apoptosome can promote oncogenic transformation *(12,14)*, although animal studies have shown that apaf-1 and caspase-9 are not tumor suppressors in myc-induced lymphomagenesis *(15)*. Apoptosome inactivation has been documented in non–small-cell lung carcinoma, melanoma, ovarian carcinoma, and leukemia cell lines *(12,16)*. Thus, apoptosis pathways are altered in some tumors, but the alteration pattern is still not clear.

In this study, we examined the status of p53, by DNA sequencing and of apoptosome activity, by measuring cytochrome c–dependent caspase activation in both human cancer cell lines and in normal human cells. We studied cancer cells that had lost p53 function but retained apoptosome function and used COMPARE analysis to identify tumor-specific, apoptosome-activating compounds. We further examined the mechanism by which one identified compound, Triacsin c, triggers the apoptosome-mediated pathway by measuring levels of cardiolipin, a phospholipid that is localized in the mitochondria and has been implicated in apoptosis regulation *(17)*, and cardiolipin function using 10-N-nonyl-acridine orange (NAO), a small compound that specifically binds to cardiolipin *(18)*. We also measured the effects of Triacsin c on the growth of xenograft lung tumors in nude mice.

Materials and Methods

Materials

Normal cell lysates were prepared from tissues obtained during surgical resection or purchased from BioChain Institute, Inc. (San Leandro, CA). Written informed consent was obtained from those patients (or their guardians) whose tissue was used in the analysis. Triacsin c was isolated as described previously *(19)* or purchased from Sigma (St. Louis, MO). SN-38 was a kind gift of Yakult (Tokyo, Japan). NAO *(18)* was purchased from Molecular Probes (Eugene, OR).

Cell Lines, Cell Culture, and Treatment

The cancer cell lines analyzed in this study were all of human origin and were used in anticancer drug screening programs at the Japanese Foundation for Cancer Research (JFCR) (Table 1). In addition, we used the p53 wild-type human cancer cell lines LoVo and LS-174T (colon), NUGC4 (stomach), YMB-1 and Mrk-nu1 (breast), and A172 and KG1C (brain). Cell lines were obtained from the National Cancer Institute (Frederick, MD) *(20)*, purchased from the American Type Culture Collection (Manassas, VA), or obtained from the Health Science Research Resources Bank (Osaka, Japan). All cancer cell lines were cultured in RPMI 1640. Normal human adult cell lines TIG108, TIG109, ASF4–1, and CCD33Co were cultured in modified Eagle medium, and the normal human adult cell line TIG114 was cultured in Eagle's basal medium. Human embryonic cell lines 293T and TIG3 were cultured in Dulbecco's modified Eagle medium or RPMI 1640, respectively. Murine fibroblast PA317 cells were grown in Dulbecco's modified Eagle medium. All culture media were supplemented with 10% heat-inactivated fetal bovine serum and 100 μg/mL of kanamycin, and cell lines were cultured in a humidified atmosphere of 5% CO_2 and 95% air at 37 °C.

For cell growth assays, cells were seeded at 2×10^4 or 5×10^4 cells/mL in 96-well plates and cultured overnight before treatment. For other analyses, cells were seeded at 1×10^5 or 2×10^5 in six-well plates or 100-mm dishes and cultured overnight before treatment. For cell growth assays, cells were treated with vehicle or 4 or 8 μ*M* Triacsin c for 48 hours; with vehicle or 1, 2, or 4 μ*M* Triacsin c for 48 hours; or with vehicle or 1 μ*M* Triacsin c for 40 hours. For assays of caspase activity, cells were treated with vehicle or 8 μ*M* Triacsin c for 30 hours, and for assays of p53 expression, cells were treated with vehicle or 8 μ*M* Triacsin c or with 3 μ*M* topoisomerase I inhibitor SN-38 for 48 hours. Triacsin c and SN-38 were dissolved in dimethyl sulfoxide (vehicle) at stock concentrations of 50 m*M* and 2 m*M*, respectively, and stored at −20 °C. The stock solutions were diluted in cell culture medium before being added to cells.

Measurement of Apoptosome Activity and Drug-Activated Caspase Activity

To determine the functional status of the apoptosome-mediated apoptosis pathway in normal and cancer cells, we measured the cytochrome c-induced activation of caspases in cell lysates. Cytosolic extracts were incubated with 10 μ*M* cytochrome c plus 1 m*M* dATP for 30 minutes, and caspase activity was measured using acetyl-Asp-Glu-Val-Asp-(4-methylcoumaryl-7-amide) (DEVD-MCA) as a substrate, as reported previously *(21)*. In brief, the cell extracts were incubated with 10 μ*M* DEVD-MCA at 37 °C for 30 minutes. The release of amino-4-methylcoumarin was monitored with a spectrofluorometer (F-2500; Hitachi, Tokyo, Japan) using an excitation wavelength of 380 nm and an emission wavelength of 460 nm. For drug-treated cells, lysates were prepared in standard buffer (10m*M* Tris-HCl, pH 8.0, 5m*M* dithiothreitol [DTT], and 1 m*M* phenylmethylsulfonyl fluoride [PMSF]) *(16)*, and caspase activity was measured as described above.

Assessment of p53 Genetic Status

p53 status of NCI-H23, NCI-H522, NCI-H460, A549, HCC-2998, KM-12, HT-29, HCT-15, LoVo, LS-174T, HCT-116,

Table 1. Apoptosome activity and p53 status in human cancer cells and normal human cells*

Cells	Apoptosome activity, RFU (95% CI)	p53 status
Lung cancer		
NCI-H23	840 (807 to 873)	Mt(M246I)
NCI-H522	1900 (1817 to 1983)	Mt(P191del)
DMS273	88 (79 to 97)	Mt(G245C)
DMS114	2300 (2192 to 2408)	Mt(R213X)
NCI-H460	170 (162 to 178)	Wild
A549	30 (24 to 36)	Wild
Colon cancer		
HCC-2998	870 (823 to 917)	Mt(R213X)
KM-12	1700 (1641 to 1759)	Mt(H179R)
HT-29	860 (805 to 915)	Mt(R273H)
HCT-15	1700 (1648 to 1752)	Mt(S241F)
LoVo	6.0 (3.1 to 8.9)	Wild
LS-174T	280 (260 to 300)	Wild
HCT-116	110 (101 to 119)	Wild
Stomach cancer		
St-4	820 (813 to 827)	Mt(Y205del)
MKN-1	590 (569 to 611)	Mt(V143A)
MKN-7	350 (330 to 370)	Mt(I251L)
MKN-28	25 (1 to 49)	Mt(I251L)
MKN-74	97 (92 to 102)	Mt(I251L)
MKN-45	100 (91 to 109)	Wild
NUGC4	22 (16 to 28)	Wild
Brain cancer		
U251	1400 (1273 to 1527)	Mt(R273H)
SF268	1600 (1424 to 1776)	Mt(R273H)
SF295	1300 (1273 to 1327)	Mt(R248Q)
SNB-75	450 (433 to 467)	Mt(E258L)
SNB-78	520 (492 to 548)	Mt(184-5del, P223A)
A172	270 (269 to 271)	Wild
KG1C	6.2 (6.0 to 6.4)	Wild
Breast cancer		
BSY-1	110.2 (109.8 to 110.6)	Mt(R248Q)
HBC-5	430 (415 to 445)	Mt(C242F)
HTB-26	2300 (2218 to 2382)	Mt(R280L)
HBC-4	16 (7 to 25)	Wild
MCF-7	9.3 (9.2 to 9.4)	Wild
YMB-1	21 (20 to 22)	Wild
Mrk-nu1	23 (22 to 24)	Wild
Normal adult cell lines		
TIG108	240.0 (239.4 to 240.6)	n.d.
TIG109	240 (217 to 263)	n.d.
ASF4–1	88 (87 to 89)	n.d.
CCD33Co	23 (22 to 24)	n.d.
TIG114	23 (22 to 24)	n.d.
Normal tissue cells		
Lung1	1.1 (1.0 to 1.2)	n.d.
Lung2	1.1 (0.6 to 1.6)	n.d.
Lung3	0.9 (0.8 to 1.0)	n.d.
Colon1	9.0 (6.1 to 11.9)	n.d.
Colon2	38 (0 to 76)	n.d.
Colon3	3.0 (2.2 to 3.8)	n.d.
Stomach1	97 (96 to 98)	n.d.
Stomach2	1.0 (0.97 to 1.03)	n.d.
Stomach3	13 (9 to 17)	n.d.
Embryonic cell lines		
293T	1400 (1327 to 1473)	n.d.
TIG3	890 (807 to 973)	n.d.

*Apoptosome activity = caspase activity, measured as described in Materials and Methods. The apoptosome activity data are the mean value of four independent experiments and are shown as relative fluorescence units (RFU). CI = confidence intervals. p53 status was determined by reverse transcription polymerase chain reaction and DNA sequencing *(23)* as in described in Materials and Methods or from previous reports *(20,22)*. wild = wild-type; Mt = mutant; del = deletion; X = termination codon; n.d. = not determined.

NUGC4, U251, SF268, SF295, SNB-75, A172, KG1C, HTB-26, MCF-7, YMB-1, and Mrk-nu1 cells has been reported previously *(20,22)*. We determined the p53 status of DMS273, DMS114, St-4, MKN-1, MKN-7, MKN-28, MKN-45, MKN-74, HBC-4, BSY-1, HBC-5, and SNB-78 cells using the method of Takahashi et al. *(23)*. In brief, we amplified p53 cDNA from the cell lines using reverse transcription polymerase chain reaction (RT-PCR) and then cloned it into the pSS16 plasmid vector. The p53 cDNA was sequenced with a Dyedeoxy terminator kit (Perkin-Elmer, Urayasu, Japan) on an ABI 373A automated sequencer (Applied Biosystems, Urayasu, Japan) according to the manufacturer's protocol.

In Silico COMPARE Analysis

The in silico COMPARE analysis was carried out as described by Yamori et al. *(24,25)*. COMPARE analysis is a calculation method to compare the pattern of enzyme activity or drug sensitivity of a test compound in a set of cancer cell lines with that of known compounds. The pattern of enzyme activity or drug sensitivity is described as a mean graph and is called a fingerprint. We have developed a database of chemosensitivities of cancer cell lines to nearly 2500 compounds, including antitumor agents and inhibitors of signal transduction.

Cell Growth Assays

The sensitivity of cell lines to Triacsin c was evaluated using the 3-(4,5-dimethylthiazol-2-yl)-5-(3-carboxymethoxyphenyl)-2-(4-sulfophenyl)-2H-tetrazolium (MTS) method *(16)*. In brief, we used CellTiter 96AQ_{ueous} One Solution Cell Proliferation Assay Kit (Promega, Tokyo, Japan). Drug-treated cells (100 μL/well in 96-well plates) were treated with 20 μL of MTS in phenazine ethosulfate solution, and the mixture was incubated at 37 °C for 30 to 60 minutes. Optical density at 490 nm was measured. Four independent experiments were performed for each cell line assayed.

Construction of Vectors

Full-length cDNAs for human caspase-9 and acyl-CoA synthetase 5 (ACSL5) were amplified by PCR. A dominant-negative form of caspase-9 (Dncaspase-9) *(14)* was generated by mutagenesis *(21)* using the QuikChange site-directed mutagenesis kit (Stratagene, La Jolla, CA), according to the manufacturer's instructions. Dncaspase-9 was cloned into the pcDNA3 vector (Invitrogen, San Diego, CA) to generate pcDNA3-Dncaspase-9-FLAG, which encodes a C-terminal FLAG epitope- agged chimeric protein. The ACSL5 gene was cloned into the pFLAG-CMV vector (Kodak, New Haven, CT) to generate pFLAG-CMV-ACSL5, which encodes a C-terminal FLAG epitope-tagged chimeric protein. For retrovirus-mediated gene transfer, Dncaspase-9-FLAG and ACSL5-FLAG were excised from pcDNA3-Dncaspase-9-FLAG and pFLAG-CMV-ACSL5, respectively, and were subcloned into the pHa-IRES-dihydrofolate reductase (DHFR) vector that we constructed previously *(26)*. The resulting vectors, pHa-Dncaspase-9-FLAG-IRES-DHFR and pHa-ACSL5-FLAG-IRES-DHFR, encoded C-terminal FLAG epitope-tagged chimeric proteins that included DHFR as a selection marker.

Transient Transfection, Retrovirus-Mediated Gene Transfer, and Inhibition of apaf-1 Expression by Small Interfering (si)RNA

To examine the roles of ACS and caspase-9 in Triacsin c–induced cell death, we first transiently transfected NCI-H23

and HCT15 cells with vectors containing chimeric ACSL5 or Dnacaspase-9 proteins and then used retrovirus-mediated gene transfer of these vectors to SF268 cells to generate stably-expressing cells.

Transient transfection was performed using Lipofectamine2000 (Invitrogen, San Diego, CA), according to the manufacturer's instructions. We co-transfected cells with pcDNA3-Dncaspase-9-FLAG and pcDNA3-enhanced green fluorescent protein (EGFP), pFLAG-CMV-ACSL5 and pcDNA3-EGFP, or their empty vectors (mock) and pcDNA3-EGFP *(27)* on day 1. After Triacsin c treatment, on day 2, cell viability was determined by counting EGFP-positive cells in samples from each transfected population.

For retrovirus-mediated gene transfer, PA317 cells were transfected with pHa-Dncaspase-9-FLAG-IRES-DHFR, pHa-ACSL5-FLAG-IRES-DHFR, or pHa-IRES-DHFR (mock), selected with methotrexate (MTX), and the conditioned media of the MTX-resistant PA317 cells was added to SF268 cells, which have high retrovirus infection efficiency, as described previously *(26)*. After retrovirus-mediated gene transfer and subsequent MTX selection (100 ng/mL), stably transduced cells were established.

siRNAs were transiently introduced into the cells with Lipofectamine2000, according to the manufacturer's instructions. The siRNA to human apaf-1 (mixture of the following four duplexes: 5′-GGACAAAUGUAUCUUUCUAUU-3′, 5′-GAACUCUGCU GUAAUGUUAUU-3′, 5′-GAACAGGUCAGAUUGAUUAUU-3′, 5′-CGACAGCCAUUUCCUAAUAUU-3′) and a nonspecific control duplex (5′-ACUCUAUCUGCACGCUGACUU-3′) were produced by Dharmacon Inc. (Chicago, IL). Twelve hours after the siRNAs were introduced, cells were reseeded at 2×10^4 cells/mL in 96-well plates and were then treated with vehicle or 2 μ*M* Triacsin c for 48 hours. Sensitivity of cells to the agent was evaluated using the MTS method, as described above.

Measurement of Acyl-CoA Synthetase Activity

Total cell lysates from mock- or ACSL5-transduced SF268 cells (treated with vehicle or 4 μ*M* Triacsin c for 48 hours) were prepared by homogenizing cells in buffer A (20 m*M* HEPES-KOH, pH 7.5, 10 m*M* KCl, 1.5 m*M* $MgCl_2$, 1 m*M* EDTA, 1 m*M* DTT, and 0.1 m*M* PMSF) *(16)*, and the acyl-CoA synthetase activity was assayed as described previously *(28)*. In brief, the assay mixture contained 1.2 μmol of $MgCl_2$, 5 μmol of ATP, 3 μmol of KF, 0.1 μmol of coenzyme A, 3 μmol of 2-mercaptoethanol, and 0.03 μmol of palmitic acid containing 0.1 μCi of [^{14}C]-palmitic acid, in a total volume of 150 μL. The reaction was initiated by adding 100 μL of cell lysate and terminated after 5 minutes at 37 °C by adding 2.25 mL of isopropanol-heptane-1 *M* H_2SO_4 (40:10:1 by volume). Then 1.5 mL of heptane and 1 mL of water were added, and the upper layer was discarded. The lower layer was washed twice with 2 mL of heptane containing 8 mg palmitic acid, and 0.1 mL of sample was counted in 1 mL of scintillation cocktail, ACSII (Amersham, Tokyo, Japan).

Measurement of Cardiolipin Levels

Cardiolipin levels were measured according to the method of Hardy et al. *(29)* with a slight modification. Mock- or ACSL5-transduced SF268 cells were labeled for 24 hours with [^{32}P]Pi (20 μCi/mL), and lipids were extracted by adding 300 μL of $CH_3OH/CHCl_3$/phosphate-buffered saline (PBS) (10:5:4), 78 μL of $CHCl_3$, and 78 μL of $CHCl_3$ and then by collecting the lower phase. Phospholipids were separated by thin-layer chromatography using silica gel plates K6 (Whatman, Tokyo, Japan), and individual species were identified by comigration of standards (Sigma-Aldrich Corp., St. Louis, MO). The cardiolipin level was determined quantitatively by exposure of autoradiography film to the lipid-separated thin-layer chromatography plates, followed by densitometric scanning of cardiolipin spots.

Isolation of Mitochondria and Estimation of Cytochrome c Release From Mitochondria

Mitochondria were isolated from SF268 cells, and cytochrome c release was examined as described *(30)*. In brief, isolated mitochondria (10 μg of protein) were incubated with NAO in a buffer containing 0.3 *M* mannitol, 10 m*M* HEPES-KOH, pH 7.4, 1 m*M* KPB, 0.1 m*M* EGTA, 0.1 m*M* EDTA, and 0.5 m*M* $MgCl_2$ for 3 hours at 37 °C. The mitochondria were centrifuged (20 000 × g) at 4 °C for 2 minutes. The supernatants were then separated by sodium dodecyl sulfate–polyacrylamide gel electrophoresis (SDS-PAGE) on 15–25% gradient gels, and cytochrome c was detected by Western blotting.

Western Blot Analysis

Monoclonal rat anti–human apaf-1 antibody (used at 1:300 dilution) was purchased from Alexis Biochemicals (San Diego, CA), monoclonal mouse anti–human cytochrome c antibody (used at 1:300 dilution) was purchased from PharMingen (San Diego, CA), monoclonal mouse anti–human tubulin antibody (used at 1:1000 dilution) and monoclonal mouse anti-FLAG antibody (used at 1:300 dilution) were purchased from Sigma, and rabbit polyclonal anti–human p53 antibody (used at 1:300 dilution) was purchased from Santa Cruz Biotechnology, Inc. Western blots were performed as described previously *(27)*. In brief, cell lysates were subjected to SDS-PAGE (4–20% or 15–25% gradient gel) and then transferred to a nitrocellulose membrane. Membranes were blocked at room temperature for 1 hour in blocking buffer (5% skim milk and 0.1% Tween-20 in PBS), incubated with the antibodies diluted as described above in blocking buffer at room temperature for 2 hours, washed three times in washing buffer (0.1 % Tween-20 in PBS), and incubated with anti–mouse, anti–rat, or anti–rabbit immunoglobulin peroxidase-conjugated antibodies (1:500 dilution; Amersham, Tokyo, Japan) at room temperature for 1 hour and washed six times with washing buffer. The bands were then visualized using ECL Western Blotting Detection Reagents (Amersham, Tokyo, Japan).

Antitumor Activity Against Xenografts

NCI-H23 cells were implanted subcutaneously in the right flank region of 9-week-old BALB/cAJcl-nu nude mice (n = 10) (Charles River Japan, Inc., Kanagawa, Japan) *(16)*. Therapeutic experiments were started approximately 10 days after implanting when tumors reached 50–150 mm^3 as measured with calipers (day 0). Triacsin c was administered by intratumoral injection in 40 μL of saline (30 $mg \cdot kg^{-1} \cdot day^{-1}$) daily on days 0, 1, and 2. Control mice (n = 5) received the same volume of saline as experimental mice (n = 5). The length (L) and width (W) of the tumor were measured, and the tumor volume (TV) was calculated

as TV = (LXWXW)/2. Tumor growth was measured for 21 days. All animal procedures were performed in the animal experiment room of the Japanese Foundation for Cancer Research (JFCR) using protocols approved by the JFCR Animal Care and Use Committee.

Statistical Analysis

All mean values and 95% confidence intervals (CIs) from at least triplicate samples were calculated with Microsoft Excel 98 software (Microsoft, Seattle, WA). Statistical significance of differences between two groups was determined with a two-sided Student *t* test using StatView software, version 4.5 (SAS Institute Inc., Cary, NC). Statistical significance of differences between two groups was also determined with Mann-Whitney's *U* test (nonparametric test) using StatView software, version 4.5. We confirmed that all the differences determined as being statistically significant with Student's *t* test were also statistically significant with Mann-Whitney's *U* test ($P<.05$, data not shown). Additionally, one-way analysis of variance with Fisher's test was also done by use of StatView software to confirm the statistical significance of differences between the apoptosome activity of normal and p53-mutant tumor cells. We calculated the degree of similarity between drug sensitivity (−log [drug concentration resulting in a 50% reduction in cell growth {GI_{50}} value of Triacsin c]) and apoptosome activity using Pearson's correlation coefficient using StatView software. For all statistical tests, *P* values of <.05 were considered statistically significant.

Results

Apoptosome-Mediated Pathway in p53-Defective Tumors

To determine if the intrinsic pathway of apoptosis was functional in cancer cells, we measured the apoptosome activity (cytochrome c–induced activation of caspases in cell lysates) of 34 human cancer cell lines, as well as in normal human adult tissue–derived cells, human adult cell lines, and human embryonic cell lines (Table 1). Most human tumor cell lines possessed elevated apoptosome activity compared with normal cells, although in some tumor cell lines, low apoptosome activity was observed (Fig. 1, A). Tumor cell lines had statistically significantly higher apoptosome activity than did normal tissue-derived cells (mean apoptosome activity of tumor cells versus that of normal tissue–derived cells; means = 626 relative fluorescence units [RFU] versus 18 RFU, respectively; difference = 608 RFU, 95% CI = 120 to 1097; $P = .016$), which is in agreement with previous reports that show elevated expression of apoptosome components in cancers *(7,8)*. In contrast with normal adult cells, which showed low apoptosome activity, embryonic cell lines showed high activity (Table 1). This higher activity may reflect the rapid growth of embryonic cells.

Because recent studies indicate that defective apoptosome component proteins play a role similar to p53 loss in promoting oncogenic transformation *(12,14)*, we examined the relationship between p53 status and apoptosome activity. We observed that tumor cell lines with defective p53 retained intact downstream apoptosome activity, whereas tumor cell lines with low apoptosome activity possessed intact p53, suggesting that a complementary pattern of p53 mutation and low apoptosome activity existed (Fig. 1, B). Tumor cells with mutant p53 retained statistically significantly elevated apoptosome activity as compared with normal tissue–derived cells (apoptosome activity of p53-mutant tumor cells versus normal tissue–derived cells; means = 964 RFU versus 18 RFU, respectively; difference = 946 RFU, 95% CI = 442 to 1450; $P<.001$) or normal adult cell lines (apoptosome activity of tumor cells versus normal adult cell lines; means = 964 RFU versus 122 RFU, respectively; difference = 842 RFU, 95% CI = 155 to 1528; $P = .018$).

In Silico COMPARE Analysis to Identify an Agent Targeting Elevated Apoptosome Activity in Tumors

We then used in silico COMPARE analysis to identify apoptosome-directing stimuli *(24,25)*. We established a human cancer cell line panel and developed a database of their chemosensitivities to nearly 2500 compounds, including antitumor agents and inhibitors of signal transduction. Drugs were profiled according to their fingerprint patterns for differential growth inhibition. Because the drug's mode of action is related to its fingerprint *(24)*, the fingerprint database can be used to predict the modes of action of new compounds and to identify compounds that target molecules involved in tumor survival. Using the COMPARE analysis, we can identify compounds in our database whose fingerprints for growth inhibition show a statistical correlation with a fingerprint of another drug or an enzyme activity *(24)*.

For this study, we designated apoptosome activity patterns of the cell lines as apoptosome fingerprints and searched for compounds in our database whose fingerprint of growth inhibition correlated well with the apoptosome pattern (Fig. 2, A). By mining our database using the COMPARE algorithm *(24)*, several candidate compounds were identified. Triacsin c, a specific inhibitor of acyl-CoA synthetase (ACS) *(19)*, had the strongest correlation between apoptosome pattern and growth inhibition. ACS catalyzes the formation of acyl-CoA from fatty acid, a reaction that is involved in both the degradation of fatty acid and the synthesis of cellular lipids. Some ACS isozymes are overexpressed in cancers *(31,32)*, which suggests that they are involved in cancer cell survival, even though their precise roles are unknown. A statistical correlation was found between apoptosome activity and the log (GI_{50} of Triacsin c) (Pearson's correlation efficient r = .589, $P = .0019$, Fig. 2, B). Moreover, Triacsin c treatment induced a statistically significant increase in cell death of those p53-defective cell lines that had high apoptosome activity [cell survival of Triacsin c–treated versus untreated H23 cells; means = 38% (8 μ*M*) or 48% (4 μ*M*) versus 100% (untreated), respectively, difference = 62% (untreated – 8 μ*M*) or 52% (untreated – 4 μ*M*), 95% CI = 60% to 65% (untreated – 8 μ*M*) or 45% to 59% (untreated – 4 μ*M*), $P<.001$; cell survival of Triacsin c–treated versus untreated DMS114 cells; means = 38% (8 μ*M*) or 38% (4 μ*M*) versus 100% (untreated), respectively, difference = 62% (untreated – 8 μ*M*) or 62% (untreated – 4 μ*M*), 95% CI = 60% to 64% (untreated – 8 μ*M*) or 59% to 64% (untreated – 4 μ*M*), $P<.001$; cell survival of Triacsin c–treated versus untreated HCT-15 cells; means = 26% (8 μ*M*) or 34% (4 μ*M*) versus 100% (untreated), respectively, difference = 74% (untreated – 8 μ*M*) or 66% (untreated – 4 μ*M*), 95% CI = 68% to 80% (untreated – 8 μ*M*) or 60% to 72% (untreated – 4 μ*M*), $P<.001$; cell survival of Triacsin c–treated versus untreated KM-12 cells; means = 53% (8 μ*M*) or 61% (4 μ*M*) versus 100% (untreated), respectively, difference = 47% (untreated – 8 μ*M*) or 39% (untreated – 4 μ*M*), 95% CI = 40% to 54% (untreated – 8 μ*M*) or 32% to 45%

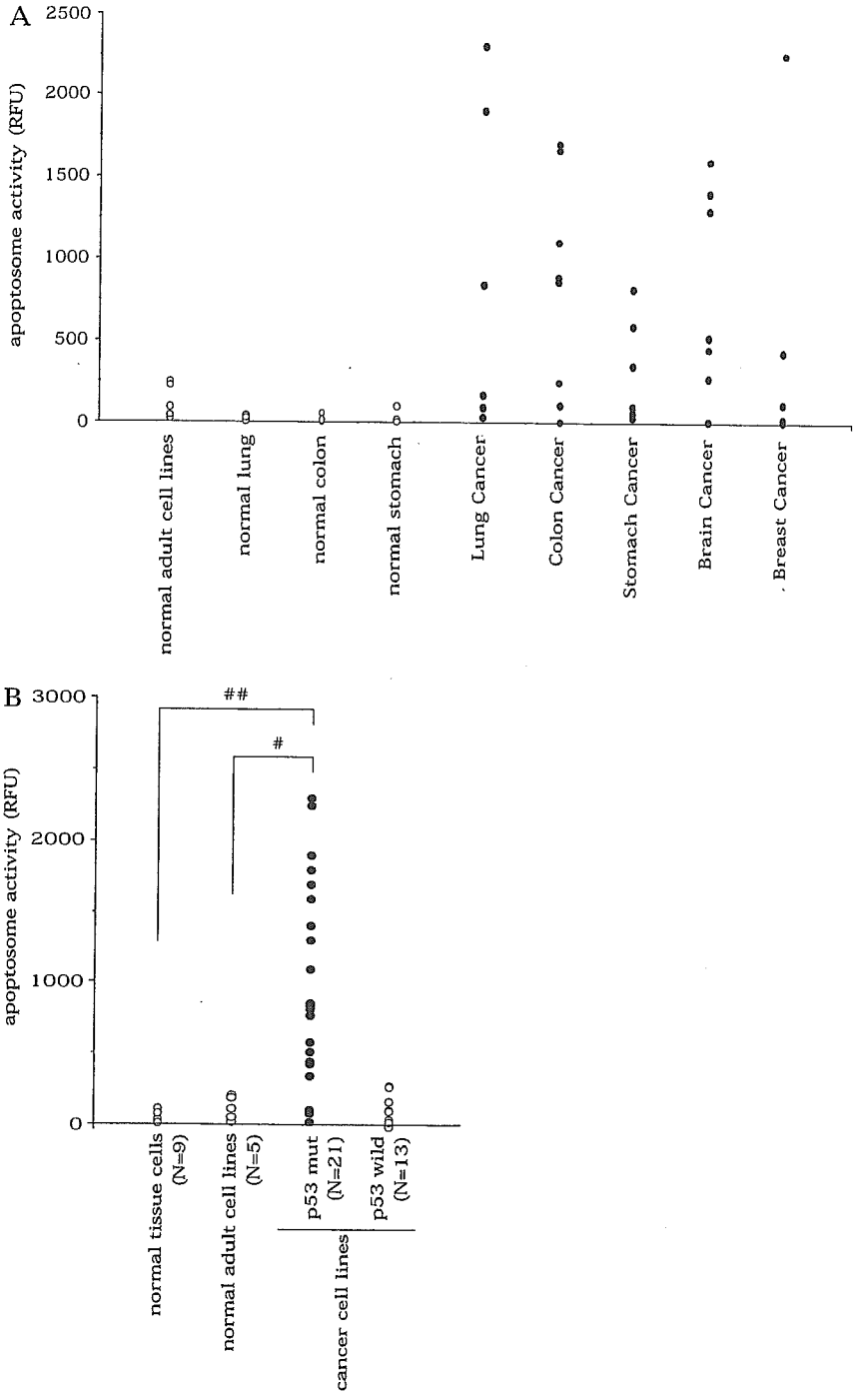

Fig. 1. Apoptosome activity in human cancer cells. **A)** Apoptosome activity in cancer cell lines compared with normal cell lines. **B)** Apoptosome activity in p53-defective tumor cell lines. Cell extracts were incubated with cytochrome c and dATP and then with acetyl-Asp-Glu-Val-Asp-(4-methyl-coumaryl-7-amide) *(21)*. The release of amino-4-methylcoumarin was monitored at 460 nm with a spectrofluorometer (F-2500; Hitachi, Tokyo, Japan). Each point represents a cell line; the activity for that line is the mean value of four independent analyses. *P* values (two-sided) were calculated using the Student *t* test. RFU = relative fluorescence units; p53 wild = p53-wild-type tumors; p53 mut = p53-mutant tumors; ##, $P<.001$; #$P = .018$.

(untreated – 4 μ*M*), $P<.001$; cell survival of Triacsin c–treated versus untreated SF268 cells; means = 48% (8 μ*M*) or 57% (4 μ*M*) versus 100% (untreated), respectively, difference = 52% (untreated – 8 μ*M*) or 43% (untreated – 4 μ*M*), 95% CI = 49% to 54% (untreated – 8 μ*M*) or 40% to 45% (untreated – 4 μ*M*), $P<.001$; cell survival of Triacsin c–treated versus untreated U251 cells; means = 35% (8 μ*M*) or 61% (4 μ*M*) versus 100% (untreated), respectively, difference = 65% (untreated – 8 μ*M*) or 39% (untreated – 4 μ*M*), 95% CI = 62% to 68% (untreated – 8 μ*M*) or 35% to 43% (untreated – 4 μ*M*), $P<.001$]. However, at the same dosage, Triacsin c was not cytotoxic to human normal cells with low apoptosome activity (Fig. 2, C).

We next examined whether Triacsin c activated the apoptosome pathway. Triacsin c induced cytochrome c release from the mitochondria, and caspase activity in treated cells was statistically significantly higher than that of untreated, untransfected NCI-H23, HCT-15, and SF268 cells (caspase activation of Triacsin c–treated versus untreated H23 cells; means = 315% versus 100%, respectively, difference = 215%, 95% CI = 209% to 221%; HCT-15 cells; means of 860% versus 100%, respectively, difference = 760%, 95% CI = 748% to 773%; SF268 cells; means = 1018% versus 100%, respectively, difference = 918%, 95% CI = 895% to 941%; $P<.001$; Fig. 3, A and B). Moreover, expression of exogenous dominant negative caspase-9 statistically significantly suppressed Triacsin c–induced cytotoxicity (cell survival of Triacsin c–treated mock- versus dominant negative caspase-9–transfected H23 cells; means = 47% versus 100%, respectively, difference = 53%, 95% CI = 47% to 59%;

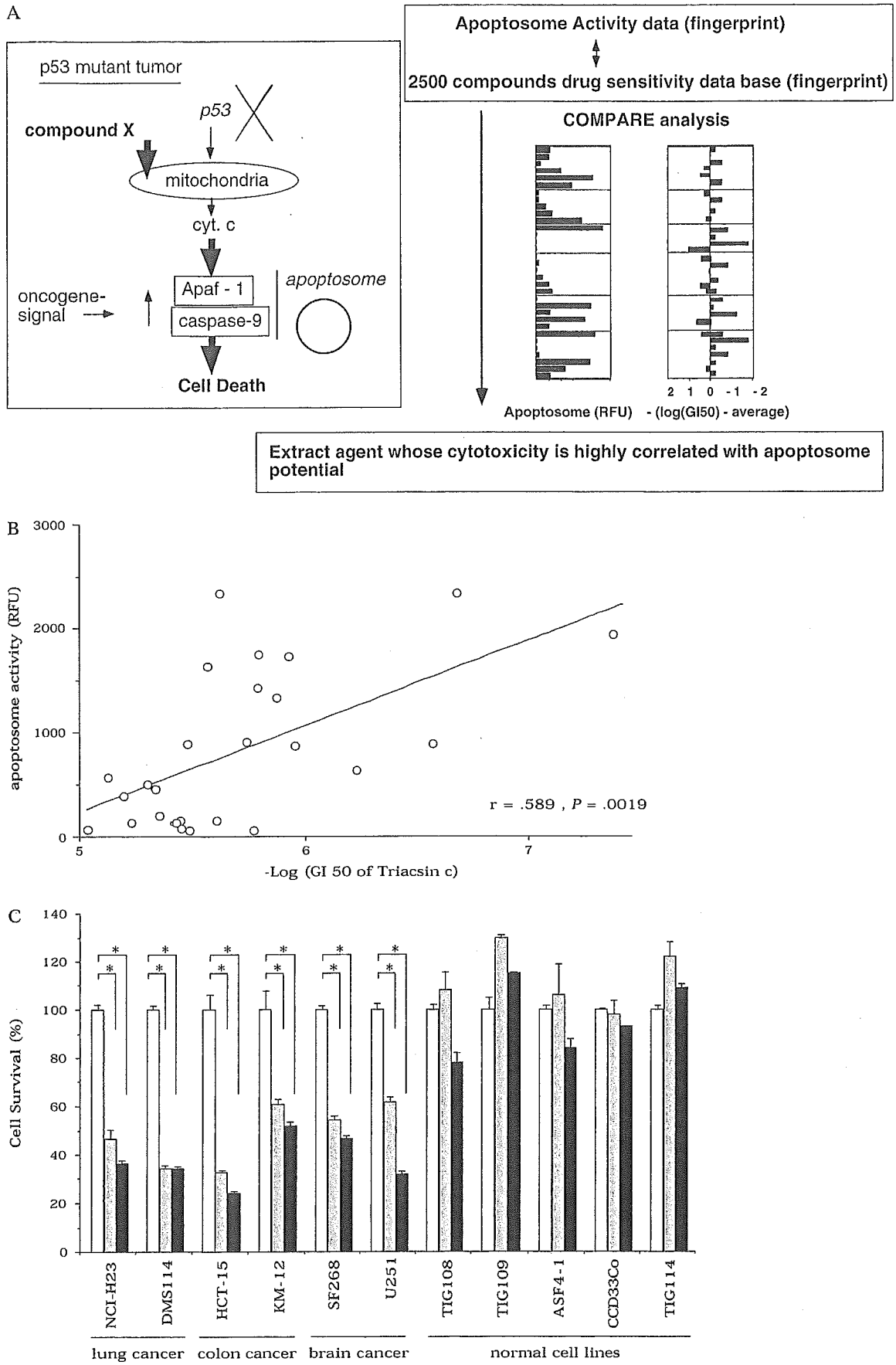

Fig. 2. Identification of agents that target cancer cells with high apoptosome activity. **A)** Strategy to identify agents that induce apoptosome-dependent death by COMPARE analysis. Cyt c = cytochrome c. **B)** Pearson's correlation of apoptosome activity (RFU = relative fluorescence units) and Triacsin c sensitivity in cancer cell lines. **C)** Sensitivity to Triacsin c of normal human cell lines with low apoptosome activity compared with that of p53-mutant tumor cell lines. Cells were treated with 0 (**open bars**), 4 (**hatched bars**), and 8 (**solid bars**) μM Triacsin c for 48 hours. We used CellTiter 96AQ$_{ueous}$ One Solution Cell Proliferation Assay Kit (Promega, Tokyo, Japan). Data shown are the mean value of three independent experiments, and error bars show 95% confidence intervals. *P* values (two-sided) were calculated using the Student *t* test. *, $P<.001$.

HCT15 cells; means of 60% versus 101%, respectively, difference = 41%, 95% CI = 24% to 58%; SF268 cells; means = 78% versus 91% [2 μ*M* Triacsin c] or 48% versus 74% [4 μ*M* Triacsin c], respectively, difference = 12% or 26%, 95% CI = 11.5% to 13.0% or 24.8% to 26.2%; $P<.001$; Fig. 3, C).

To further determine whether Triacsin c was acting specifically on the apoptosome, we used siRNA to knock down apaf-1, the main apoptosome component. Apaf-1 knockdown statistically significantly inhibited cell death (cell survival of Triacsin c–treated control versus apaf-1 siRNA-transfected cells; means = 70% [untransfected] or 73% [control siRNA-transfected] versus 91%, respectively, difference = 21% or 18%, 95% CI = 17% to 26% or 15% to 21%; $P<.001$; Fig. 3, D). In addition, in normal TIG109 cells, Triacsin c did not induce p53 expression, whereas the topoisomerase I inhibitor SN-38 induced p53 accumulation (Fig. 3, E).

Involvement of ACS in Tumor Cell Survival and the Maintenance of Cardiolipin Level

To determine the biologic significance of Triacsin c–mediated ACS inhibition in cell death, we expressed ACSL5, a Triacsin c–resistant ACS isozyme *(33)*, in NCI-H23, HCT-15, and SF268 cancer cells (Fig. 4, A), which restored the ACS activity that decreased with Triacsin c treatment. The expression of ACSL5 statistically significantly inhibited Triacsin c–induced cell death (cell survival of Triacsin c–treated mock- versus ACSL5-transfected H23 cells; means = 51% versus 114%, respectively, difference = 63%, 95% CI = 54% to 71%; HCT15 cells; means = 67% versus 102%, respectively, difference = 35%, 95% CI = 28% to 42%; $P<.001$; Fig. 4, B, left). Retrovirus-mediated gene transfer confirmed that the stable expression of ACSL5 prevented Triacsin c–induced decreased ACS activity (ACS activity of Triacsin c–treated mock- versus ACSL5-transduced SF268 cells; means = 41% versus 165%, respectively, difference = 124%, 95% CI = 120% to 128%, $P<.001$; Fig. 4, D) and strongly inhibited cell death (cell survival of Triacsin c–treated mock- versus ACSL5-transduced SF268 cells; means = 76% versus 91% (2 μ*M* Triacsin c) or 40% versus 83% (4 μ*M* Triacsin c), respectively, difference = 15% or 43%, 95% CI = 14% to 16% or 39% to 47%; $P<.001$; Fig. 4, B, right; Fig. 4, C). Moreover, the expression of ACSL5 suppressed cytochrome c release and subsequent caspase activation (caspase activation of Triacsin c–treated mock- versus ACSL5-transduced SF268 cells; means = 705% versus 95% (24 hours) or 7780% versus 740% (48 hours), respectively, difference = 610% or 7040%, 95% CI = 587% to 633% or 6900% to 7100%; $P<.001$; Fig, 4, E and F).

Several lines of evidence indicate that cardiolipin, a mitochondrial phospholipid, interacts with cytochrome c and is involved in retaining cytochrome c in the mitochondria *(17)*. Because acyl-CoA is required for phospholipid biosynthesis, we examined whether the cardiolipin level could be modified by ACS inhibition. The total phospholipid level in untransfected SF268 cells decreased gradually after ACS inhibition by Triacsin c (total phospholipid level of Triacsin c–treated versus untreated mock-transfected cells; means = 75.5% versus 100%, respectively, difference = 24.5%, 95% CI = 23.7% to 25.3%, $P<.001$; Fig. 5, A), and the cardiolipin level decreased statistically significantly. Cardiolipin levels were restored upon ACSL5 expression (cardiolipin level of Triacsin c–treated versus untreated mock-transfected cells; means = 63% versus 100%, respectively, difference = 37%, 95% CI = 24% to 50%, $P = .0013$ for 24 hours of treatment; means = 36% versus 100%, respectively, difference = 64%, 95% CI = 58% to 70%; $P<.001$ for 48 hours of treatment; Fig. 5, B).

To determine the link between cardiolipin levels and cytochrome c release, we tested the effect of NAO on mitochondria isolated from untransfected SF268 cells. NAO binds specifically to cardiolipin, preventing it from interacting with its binding proteins *(18)*. After treatment with NAO, cytochrome c was released from the mitochondria (Fig. 5, C). Thus, cardiolipin is involved in cytochrome c release.

In Vivo Antitumor Activity of Triacsin c Against Human Cancer Xenografts

To evaluate the role of ACS in tumor cell survival in vivo, we inoculated nude mice with NCI-H23 human lung cancer cells. We used this line because the cells have high apoptosome activity and grow stably in nude mice. Once tumors reached 50–150 mm^3, they were treated with Triacsin c. Triacsin c statistically significantly inhibited the growth of tumor xenografts from day 7 to 21 (relative tumor volume of Triacsin c–treated versus untreated group; means = 1.6 versus 2.2 (day 7), 2.1 versus 3.6 (day 11), 2.8 versus 5.6 (day 14), 3.7 versus 7.9 (day 18), and 4.6 versus 9.6 (day 21), respectively; difference = 0.6 (day 7), 1.5 (day 11), 2.8 (day 14), 4.2 (day 18), and 5.0 (day 21); 95% CI = 0.052 to 1.10 (day 7), 0.32 to 2.6 (day 11), 0.90 to 4.86 (day 14), 1.4 to 6.8 (day 18), and 2.1 to 7.9 (day 21); $P = .0359$ (day 7), .0207 (day 11), .0118 (day 14), .0098 (day 18), and .0059 (day 21); Fig. 6, upper panel), compared with tumors in untreated mice. We observed no decrease in body weight of the Triacsin c–treated mice compared with that of untreated mice throughout these experiments (Fig. 6, lower panels).

Discussion

The activity of the apoptosome-mediated pathway, the intrinsic machinery of apoptosis, was elevated in the majority of tumor cells examined but was low in some tumor cells, compared with normal cells. Moreover, we observed a complementary pattern between p53 loss and low apoptosome activity in human cancer cell lines. Here, we applied an in silico COMPARE approach *(24,25)* and successfully identified Triacsin c, a specific inhibitor of ACS, as an agent that selectively targets the apoptosome pathway of tumor cells. Restoration of ACS activity by the expression of ACSL5 suppressed Triacsin c–induced cell death, indicating that ACS inhibition was a critical step for the tumor-selective activation of the apoptosome pathway. Moreover, we showed that ACS was involved in the maintenance of levels of cardiolipin, a mitochondrial phospholipid that anchors cytochrome c and that ACS inhibition induced cytochrome c release.

The results in this study agree with data from previous studies that show the complementary role of apoptosome inactivation and p53 loss in tumor growth *(12,14)*. Scott et al. *(15)* report, however, that, unlike loss of p53, loss of apaf-1 alone is not enough to promote oncogene-induced transformation of mouse embryo fibroblasts. One explanation could be that, in the apoptosome-defective cancer cells, additional defects occur that promote malignant transformation.

Our data indicate that most p53-mutated tumors retain apoptosome activity and that it is higher in tumor cells than in normal cells. This finding provides a molecular basis for clinical trials of

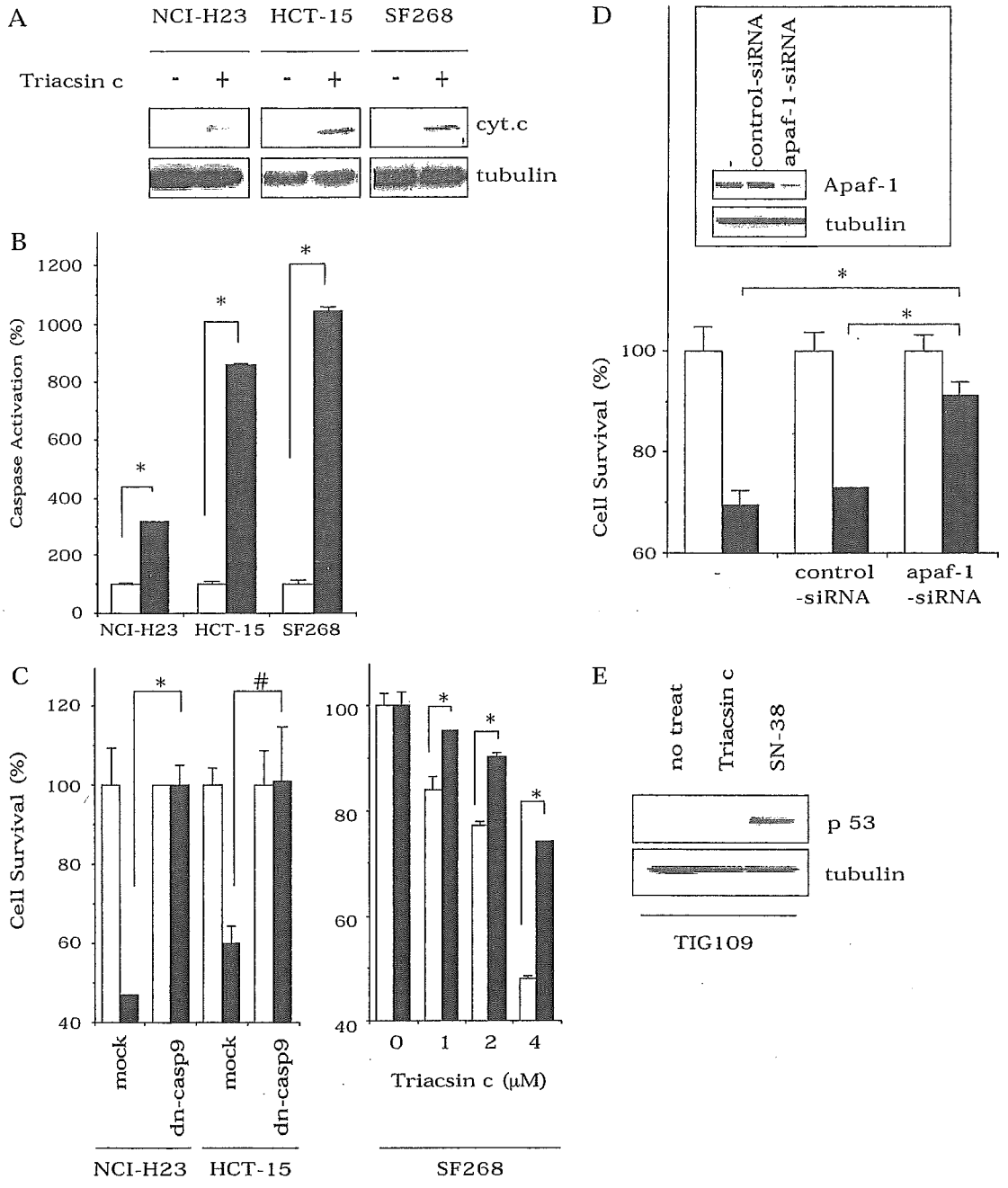

Fig. 3. Apoptosome-mediated cell death after treatment with Triacsin c, after transfection with dominant negative caspase-9 (dn-casp9), and after apaf-1 knockdown. For **A)** cytochrome c release and **B)** caspase activation assays, human lung cancer NCI-H23, human colon cancer HCT-15, and human glioma SF268 cells were treated with 0 μM (**open bars**) or 8 μ*M* (**solid bars**) Triacsin c for 30 hours. Cytochrome c release was detected by Western blot using a monoclonal mouse anti–human cytochrome c antibody (PharMingen, San Diego, CA). Total protein loading was evaluated by blotting with a monoclonal mouse anti–human tubulin antibody (Sigma, St. Louis, MO). Caspase activity was measured using acetyl-Asp-Glu-Val-Asp-(4-methyl-coumaryl-7-amide) as a substrate. **C)** Mock-transfected or dominant negative-caspase 9-transfected NCI-H23 and HCT-15 cells were treated with 0 (**open bars**) μ*M* or 1 (**solid bars**) μ*M* Triacsin c for 40 hours. Mock-transfected (**open bars**) or dominant negative-caspase 9-transfected (**solid bars**) SF268 cells were treated with 0, 1, 2, or 4 μ*M* Triacsin c for 48 hours. Transient transfection of NCI-H23 and HCT-15 cells was performed using Lipofectamine2000 (Invitrogen, San Diego, CA). In SF268 cells, stably transduced cells were established by retrovirus-mediated gene transfer, using retrovirus vectors, pHa-Dncaspase-9-FLAG-IRES-DHFR, or pHa-IRES-DHFR (mock). Sensitivity of cells to Triacsin c was evaluated using the CellTiter 96AQ$_{ueous}$ One Solution Cell Proliferation Assay Kit (Promega, Tokyo, Japan), and optical density at 490 nm was measured. **D)** Ninety-six hours after SF268 cells were transfected with small interfering (si) RNA, cytosolic fractions were prepared to examine apaf-1 expression by Western blot using a monoclonal rat anti–human apaf-1 antibody (Alexis Biochemicals, San Diego, CA), or cells were treated with 0 (**open bars**) μM or 2 (**solid bars**) μ*M* Triacsin c for 48 hours. Data shown are the mean values of three independent experiments, and error bars show 95% confidence intervals. *P* values (two-sided) were calculated using the Student *t* test (*, $P<.001$; #, $P=.0024$. **E)** p53 expression in normal human TIG109 cells as determined by Western blot with rabbit polyclonal anti–human p53 antibody (Santa Cruz Biotechnology, San Cruz, CA). Total protein loading was evaluated by blotting with a monoclonal mouse anti–human tubulin antibody. Cells were untreated (no treat) or treated with 8 μ*M* Triacsin c or with 3 μ*M* topoisomerase I inhibitor SN-38 for 48 hours.

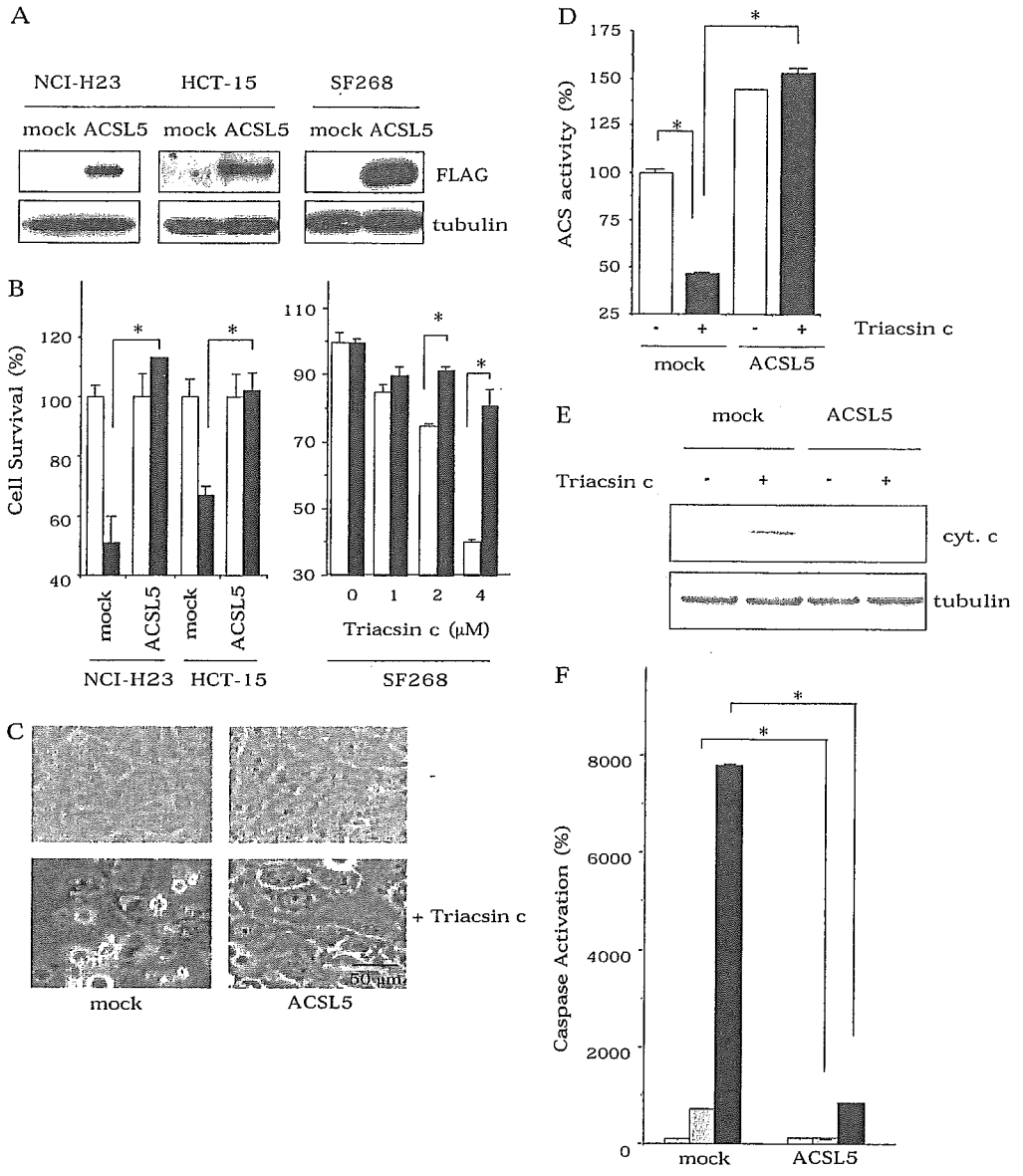

Fig. 4. Involvement of acyl-CoA synthetase (ACS) in the retention of cytochrome c in the mitochondria. **A)** The expression of FLAG epitope-tagged acyl-CoA synthetase 5 (ACSL5) in transfected cells by Western blot with monoclonal mouse anti-FLAG antibody (Sigma, St. Louis, MO). Total protein loading was evaluated by blotting with a monoclonal mouse anti–human tubulin antibody (Sigma). **B)** Cell death after Triacsin c treatment. Mock-transfected or ACSL5-transfected NCI-H23 and HCT-15 cells were treated with 0 (**open bars**) μ*M* or 1 (**solid bars**) μ*M* Triacsin c for 40 hours. In SF268 cells, mock-transduced (**open bars**) or ACSL5-transduced (**solid bars**) cells were treated with 0 μ*M*, 1 μ*M*, 2 μ*M*, or 4 μ*M* Triacsin c for 48 hours. We used CellTiter 96AQ$_{ueous}$ One Solution Cell Proliferation Assay Kit (Promega, Tokyo, Japan), and optical density at 490nm was measured. **C)** Apoptotic morphologic changes following Triacsin c treatment in mock-transduced and ACSL5-transduced SF268 cells. **D)** ACS activity following Triacsin c treatment in mock-transduced and ACSL5-transduced SF268 cells. The ACS assay was performed as described previously *(28)* and as in Materials and Methods. **E)** Cytochrome c release as measured by Western blot using a monoclonal mouse anti–human cytochrome c antibody (PharMingen, San Diego, CA). Total protein loading was evaluated by blotting with a monoclonal mouse anti–human tubulin antibody (Sigma, St. Louis, MO) and **F)** caspase activation in mock-transduced and ACSL5-transduced SF268 cells. Caspase activity was measured by incubating with 10 μ*M* acetyl-Asp-Glu-Val-Asp-(4-methyl-coumaryl-7-amide) and measuring the release of amino-4-methylcoumarin at 460 nm using a spectrofluorometer (F-2500; Hitachi, Tokyo, Japan). SF268 cells were untreated or treated with 4 μ*M* Triacsin c for 36 hours (**C**), for 24 hours (**D,E**) or for 0 (**open bars**), 24 (**hatched bars**) and 48 (**solid bars**) hours (**F**). Data are the mean values of three independent experiments, and error bars show 95% confidence intervals. *P* values (two-sided) were calculated using the Student *t* test (*, $P<.001$).

patients with p53 mutant tumors by wild-type p53 gene transfer or the downstream gene transfer therapy. Furthermore, our data raise the possibility that stimuli that bypass the p53 defect and activate the downstream apoptosome directly could selectively kill p53-mutant tumor cells.

The main limitation of our study is that our results are based on the data from a representative set of human cancer cell lines. Further studies are needed to validate our result in a larger set of cancer cells, including those from tumor samples.

Our results indicate that ACS promotes cancer cell survival by maintaining cardiolipin level and cytochrome c retention in the mitochondria and that ACS inhibition leads to the activation of the apoptosome-mediated pathway. Moreover, NAO, a specific cardiolipin inhibitor, induced cytochrome c release (Fig. 5, C), and this finding suggests that lowered cardiolipin level causes cytochrome c release in ACS inhibition–induced cell death (Fig. 7). Previous reports have demonstrated, in liposomes formed from defined lipid mixtures with a composition similar to that of

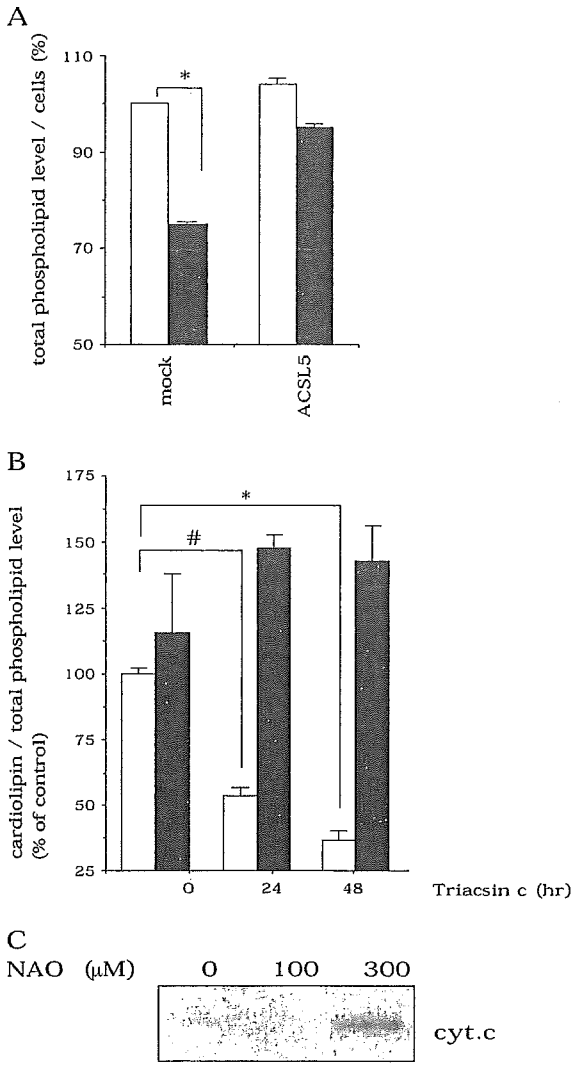

Fig. 5. Involvement of cardiolipin in mitochondrial cytochrome c release. **A)** Change in total phospholipid level after Triacsin c treatment. Mock-transduced or ACSL5-transduced SF268 cells were left untreated (**open bars**) or treated with 4 μM Triacsin c (**solid bars**) for 24 hours. Total phospholipid levels were measured as described in Materials and Methods. **B)** Change in cardiolipin content per total phospholipid after Triacsin c treatment. Mock-transduced (**open bars**) or ACSL5-transduced (**solid bars**) SF268 cells were left untreated or treated with 4 μM Triacsin c for 24 and 48 hours. Data shown are the mean value of three independent experiments, and error bars show 95% confidence intervals. *P* values (two-sided) were calculated using the Student *t* test. *, $P<.001$; #, $P = .0013$. **C)** Cytochrome c release from isolated mitochondria following 10-N-nonyl-acridine orange (NAO) treatment. Mitochondria were isolated from SF268 cells as described *(30)* and treated as described in Materials and Methods. Cytochrome c was detected by Western blot using a monoclonal mouse anti–human cytochrome c antibody (PharMingen, San Diego, CA).

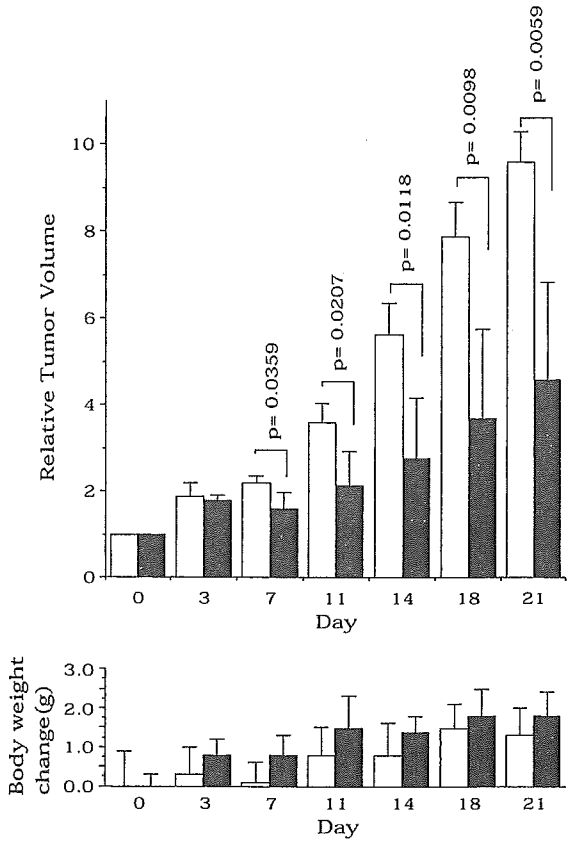

Fig. 6. Effect of acyl-CoA synthetase (ACS) inhibitor on tumor growth and body weight change in nude mice bearing human cancer xenografts. Therapeutic experiments were started (day 0) when tumors reached 50–150 mm^3. Triacsin c was administered by intratumoral injection in 40 μL of solution (30 $mg \cdot kg^{-1} \cdot day^{-1}$) daily from days 0 to 2. Control mice received the same volume of saline as did experimental mice. The length (L) and width (W) of the tumor were measured, and the tumor volume (TV) was calculated as TV = (LXWXW)/2. The **open bars** represent the control group, whereas **solid bars** represent the Triacsin c–treated group. Bars depict the mean values of five mice, and error bars show 95% confidence intervals. *P* values (two-sided) were calculated using the Student *t* test.

mitochondria of eggs of the amphibian *Xenopus laevis*, that cardiolipin is also involved in proapoptotic steps by cooperating with Bid and Bax *(34)*, although contrasting results were presented from a study using yeast mitochondria *(35)*. Thus, further studies are needed to clarify the role of cardiolipin in the apoptosis of human cancer cells.

Our results showed that blocking cardiolipin function is one way to initiate the intrinsic apoptosis pathway. However, alternative mechanisms should also be considered in ACS inhibition–induced apoptosis, because acyl-CoA is involved in multiple biochemical pathways, including adenine nucleotide translocase regulation and beta-oxidation. It has been suggested that adenine nucleotide translocase plays a role in cytochrome c release from the mitochondria during apoptosis *(36)*. Because acyl-CoA inhibits adenine nucleotide translocase *(37)*, we hypothesize that ACS inhibition could lead to a decrease in intracellular acyl-CoA levels, activation of adenine nucleotide translocase, and, subsequently, to the release of cytochrome c through activated adenine nucleotide translocase. Recent evidence against the involvement of adenine nucleotide translocase in cytochrome c release *(38)* could discount this hypothesis, though. Because acyl-CoA also interacts with other mitochondrial proteins *(39)*, additional studies are required to define the role of these interactions in apoptosis.

ACS catalyzes the formation of acyl-CoA from fatty acid, a critical step in fatty acid degradation through beta-oxidation, and the inhibition of ACS causes the accumulation of free fatty acid *(40)*. Because free fatty acid has the potential to promote the opening of the mitochondrial permeability transition pore *(41)* or to cause cytochrome c release *(42)*, the accumulation of free fatty acid could be another mechanism to initiate apoptosome pathway by ACS inhibition.

The precise role of ACS in fatty acid biosynthesis is still undefined. However, it is known that ACSL5 localizes mainly to the mitochondria *(33)* and is overexpressed in glioma *(31)*. Our

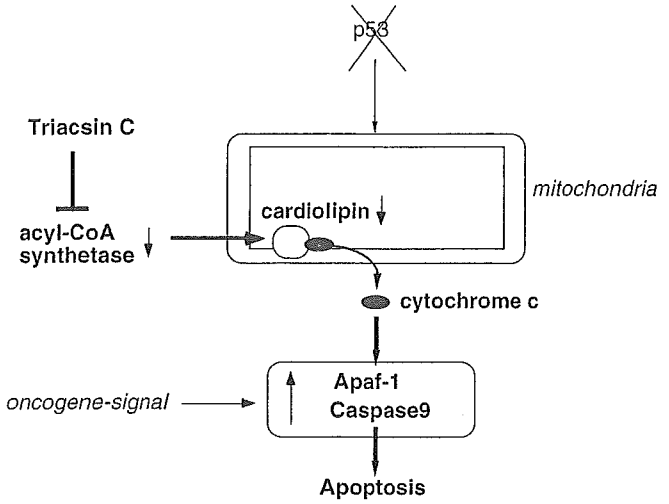

Fig. 7. Possible model for the regulation of mitochondrial cardiolipin by acyl-CoA synthetase, inhibition of which leads to preferential apoptosome-mediated tumor cell death.

results indicate that the ACSL5 isozyme plays a dominant role in biosynthesis of mitochondrial cardiolipin and could be involved in cancer cell survival.

In this study, we observed that ACS inhibition preferentially induced apoptosome-mediated death of cancer cells, and we identified Triacsin c as a specific activator of this pathway. Although p53 induces apaf-1 transcription in cancer cells *(5)*, in our study, Triacsin c did not induce p53 expression in normal cells, which may explain why the agent is less toxic to normal cells. Triacsin c also suppressed growth of tumor xenografts without any decrease in body weight of the murine host. Taken together with the frequent expression of ACS in human cancers *(31,32)*, we suggest that ACS may be a good target for chemotherapy. However, further studies are needed to define the specific role of each ACS isozyme in malignant transformation.

References

(1) Strasser A, O'Connor L, Dixit, V. Apoptosis signaling. Annu Rev Biochem 2000;69:217–45.

(2) Budihardjo I, Oliver H, Lutter M, Luo X, Wang X. Biochemical pathways of caspase activation during apoptosis. Annu Rev Cell Dev Biol 1999;15: 269–90.

(3) Fridman JS, Lowe SW. Control of apoptosis by p53. Oncogene 2003;22:9030–40.

(4) Fearnhead HO, Rodriguez J, Govek EE, Guo W, Kobayashi R, Hannon G, et al. Oncogene-dependent apoptosis is mediated by caspase-9. Proc Natl Acad Sci U S A 1998;95:13664–9.

(5) Moroni MC, Hickman ES, Denchi EL, Caprara G, Colli E, Cecconi F, et al. Apaf-1 is a transcriptional target for E2F and p53. Nat Cell Biol 2001;3: 552–8.

(6) Nahle Z, Polakoff J, Davuluri RV, McCurrach ME, Jacobson MD, Narita M, et al. Direct coupling of the cell cycle and cell death machinery by E2F. Nat Cell Biol 2002;4:859–64.

(7) Vakkala M, Paakko P, Soini Y. Expression of caspases 3, 6 and 8 is increased in parallel with apoptosis and histological aggressiveness of the breast lesion. Br J Cancer 1999;81:592–99.

(8) Krepela E, Prochazka J, Liul X, Fiala P, Kinkor Z. Increased expression of Apaf-1 and procaspase-3 and the functionality of intrinsic apoptosis apparatus in non–small-cell lung carcinoma. Biol Chem 2004;385:153–68.

(9) Mendelsohn AR, Hamer JD, Wang ZB, Brent R. Cyclin D3 activates Caspase 2, connecting cell proliferation with cell death. Proc Natl Acad Sci U S A 2002;99:6871–6.

(10) Nguyen JT, Wells JA. Direct activation of the apoptosis machinery as a mechanism to target cancer cells. Proc Natl Acad Sci U S A 2003;100:7533–8.

(11) Fantin VR, Berardi MJ, Scorrano L, Korsmeyer SJ, Leder PA. Novel mitochondriotoxic small molecule that selectively inhibits tumor cell growth. Cancer Cell 2002;2:29–42.

(12) Johnstone RW, Ruefli AA, Lowe SW. Apoptosis: a link between cancer genetics and chemotherapy. Cell 2002;108:153–64.

(13) Tsuruo T, Naito M, Tomida A, Fujita N, Mashima T, Sakamoto H, Haga N. Molecular targeting therapy of cancer: drug resistance, apoptosis and survival signal. Cancer Sci 2003;94:15–21.

(14) Schmitt CA, Fridman JS, Yang M, Baranov E, Hoffman RM, Lowe SW. Dissecting p53 tumor suppressor functions in vivo. Cancer Cell 2002;1:289–98.

(15) Scott CL, Schuler M, Marsden VS, Egle A, Pellegrini M, Nesic D, et al. Apaf-1 and caspase-9 do not act as tumor suppressors in myc-induced lymphomagenesis or mouse embryo fibroblast transformation. J Cell Biol 2004;164:89–96.

(16) Yang L, Mashima T, Sato S, Mochizuki M, Sakamoto H, Yamori T, et al. Predominant suppression of apoptosome by inhibitor of apoptosis protein in non–small-cell lung cancer H460 cells: therapeutic effect of a novel polyarginine-conjugated Smac peptide. Cancer Res 2003;63:831–7.

(17) Iverson SL, Orrenius S. The cardiolipin-cytochrome c interaction and the mitochondrial regulation of apoptosis. Arch Biochem Biophys 2004;423:37–46.

(18) Kim TH, Zhao Y, Ding WX, Shin JN, He X, Seo YW, et al. Bid-cardiolipin interaction at mitochondrial contact site contributes to mitochondrial cristae reorganization and cytochrome C release. Mol Biol Cell 2004;15:3061–72.

(19) Tomoda H, Igarashi K, Omura S. Inhibition of acyl-CoA synthetase by triacsins. Biochim Biophys Acta 1987;921:595–8.

(20) O'Connor PM, Jackman J, Bae I, Myers TG, Fan S, Mutoh M, et al. Characterization of the p53 tumor suppressor pathway in cell lines of the National Cancer Institute anticancer drug screen and correlations with the growth-inhibitory potency of 123 anticancer agents. Cancer Res 1997;57:4285–300.

(21) Sakamoto H, Mashima T, Yamamoto K, Tsuruo T. Modulation of heat-shock protein 27 (Hsp27) anti-apoptotic activity by methylglyoxal modification. J Biol Chem 2002;277:45770–5.

(22) Jia LQ, Osada M, Ishioka C, Gamo M, Ikawa S, Suzuki T, et al. Screening the p53 status of human cell lines using a yeast functional assay. Mol Carcinog 1997;19:243–53.

(23) Takahashi M, Tonoki H, Tada M, Kashiwazaki H, Furuuchi K, Hamada J, et al. Distinct prognostic values of p53 mutations and loss of estrogen receptor and their cumulative effect in primary breast cancers. Int J Cancer 2000;89:92–9.

(24) Yamori T. Panel of human cancer cell lines provides valuable database for drug discovery and bioinformatics. Cancer Chemother Pharmacol 2003;52:S74–9.

(25) Yamori T, Matsunaga A, Sato S, Yamazaki K, Komi A, Ishizu K, et al. Potent antitumor activity of MS-247, a novel DNA minor groove binder, evaluated by an in vitro and in vivo human cancer cell line panel. Cancer Res 1999;59:4042–9.

(26) Kage K, Tsukahara S, Sugiyama T, Asada S, Ishikawa E, Tsuruo T, et al. Dominant-negative inhibition of breast cancer resistance protein as drug efflux pump through the inhibition of S-S dependent homodimerization. Int J Cancer 2002;97:626–30.

(27) Mashima T, Naito M, Tsuruo T. Caspase-mediated cleavage of cytoskeletal actin plays a positive role in the process of morphological apoptosis. Oncogene 1999;18:2423–30.

(28) Banis RJ, Tove SB. Solubilization of a long chain fatty acyl-CoA synthetase from chicken adipose tissue microsomes. Biochim Biophys Acta 1974;348:210–20.

(29) Hardy S, El-Assaad W, Przybytkowski E, Joly E, Prentki M, Langelier Y. Saturated fatty acid-induced apoptosis in MDA-MB-231 breast cancer cells. A role for cardiolipin. J Biol Chem 2003;278:31861–70.

(30) Shimizu S, Tsujimoto Y. Proapoptotic BH3-only Bcl-2 family members induce cytochrome c release, but not mitochondrial membrane potential loss, and do not directly modulate voltage-dependent anion channel activity. Proc Natl Acad Sci U S A 2000;97:577–82.

(31) Yamashita Y, Kumabe T, Cho YY, Watanabe M, Kawagishi J, Yoshimoto T, et al. Fatty acid induced glioma cell growth is mediated by the acyl-CoA synthetase 5 gene located on chromosome 10q25.1-q25.2, a region frequently deleted in malignant gliomas. Oncogene 2000;19:5919–25.

(32) Cao Y, Dave KB, Doan TP, Prescott SM. Fatty acid CoA ligase 4 is up-regulated in colon adenocarcinoma. Cancer Res 2001;61:8429–34.

(33) Coleman RA, Lewin TM, Van Horn CG, Gonzalez-Baro MR. Do long-chain acyl-CoA synthetases regulate fatty acid entry into synthetic versus degradative pathways? J Nutr 2002;132:2123–6.
(34) Kuwana T, Mackey MR, Perkins G, Ellisman MH, Latterich M, Schneiter R, et al. Bid, Bax, and lipids cooperate to form supramolecular openings in the outer mitochondrial membrane. Cell 2002;111:331–42.
(35) Iverson SL, Enoksson M, Gogvadze V, Ott M, Orrenius S. Cardiolipin is not required for Bax-mediated cytochrome c release from yeast mitochondria. J Biol Chem 2004;279:1100–7.
(36) Marzo I, Brenner C, Zamzami N, Jurgensmeier JM, Susin SA, Vieira HL, et al. Bax and adenine nucleotide translocator cooperate in the mitochondrial control of apoptosis. Science 1998;281:2027–31.
(37) Woldegiorgis G, Yousufzai SY, Shrago E. Studies on the interaction of palmitoyl coenzyme A with the adenine nucleotide translocase. J Biol Chem 1982;257:14783–7.
(38) Kokoszka JE, Waymire KG, Levy SE, Sligh JE, Cai J, Jones DP, et al. The ADP/ATP translocator is not essential for the mitochondrial permeability transition pore. Nature 2004;427:461–5.
(39) Woldegiorgis G, Lawrence J, Ruoho A, Duff T, Shrago E. Photoaffinity labeling of mitochondrial proteins with 2-azido [32P]palmitoyl CoA. FEBS Lett 1995;364:143–6.
(40) Arai T, Kawakami Y, Matsushima T, Okuda Y, Yamashita K. Intracellular fatty acid downregulates ob gene expression in 3T3-L1 adipocytes. Biochem Biophys Res Commun 2002;297:1291–6.
(41) Wieckowski MR, Brdiczka D, Wojtczak L. Long-chain fatty acids promote opening of the reconstituted mitochondrial permeability transition pore. FEBS Lett 2000;484:61–4.
(42) Scorrano L, Penzo D, Petronilli V, Pagano F, Bernardi P. Arachidonic acid causes cell death through the mitochondrial permeability transition. Implications for tumor necrosis factor-alpha apoptotic signaling. J Biol Chem 2001;276:12035–40.

NOTES

This work was supported by a grant-in-aid for cancer research from the Ministry of Education, Culture, Sports, Science and Technology of Japan. We thank Dr. S. Ohyama for assistance in the measurement of apoptosome activity of normal human cells.

Manuscript received October 25, 2004; revised March 11, 2005; accepted April 5, 2005.